Received: 25 March 2024 | Revised: 12 August 2024 | Accepted: 21 August 2024

DOI: 10.1002/mma.10464

RESEARCH ARTICLE

WILEY

Product integration techniques for fractional integro-differential equations

Sunil Kumar | **Poonam Yadav** | **Vineet Kumar Singh**

Department of Mathematical Sciences, Indian Institute of Technology, Banaras Hindu University, Varanasi, India

Correspondence
Vineet Kumar Singh, Department of Mathematical Sciences, Indian Institute of Technology, Banaras Hindu University, Varanasi 221005, India.
Email: vksingh.mat@iitbhu.ac.in

Communicated by: I. Nizovtseva

Funding information
The first author is grateful for the funding provided by the Senior Research Fellow (SRF) programme of the University Grants Commission (UGC), India, and the third author acknowledges the financial support from the Council of Science and Technology, U.P. under the project ID:1893.

This article presents an application of approximate product integration (API) to find the numerical solution of fractional order Volterra integro-differential equation based on Caputo non-integer derivative of order ν, where $0 < \nu < 1$. Also, the idea is extended to a class of fractional order Volterra integro-differential equation with a weakly singular kernel. For this purpose, two numerical schemes are established by utilizing the concept of the API method, and L1 and L1-2 formulae. We applied L1 and L1-2 discretization to approximate the Caputo non-integer derivative. At the same time, Taylor's series expansion of an unknown function is taken into consideration when approximating the Volterra part in the considered mathematical model using the API method. Combination of API method with L1 and L1-2 formula provided the order of convergence $(2 - \nu)$ and $(3 - \nu)$ for Scheme-I and Scheme-II, respectively. The derived techniques reduced the proposed model to a set of algebraic equations that can be resolved using well-known numerical algorithms. Furthermore, the unconditional stability, convergence, and numerical stability of the formulated schemes have been rigorously investigated. Finally, we conducted some numerical experiments to validate our theoretical findings and guarantee the accuracy and efficiency of the recommended schemes. The comparison between the numerical outcomes obtained by proposed schemes and existing numerical techniques has also been provided through tables and graphs.

KEYWORDS

API method, Caputo non-integer derivative, integro-differential equations of Volterra type, L1 and L1-2 approximation, stability and convergence analysis

MSC CLASSIFICATION

65D25, 65D30, 45J05, 26A33

1 | INTRODUCTION

Fractional calculus allows for the computation of integrals and derivatives of arbitrary order. The field of fractional calculus, which studies mathematical theories related to fractions, has a rich and extensive history that dates back thousands of years. Different researchers and prominent mathematicians like Leibniz, Euler, and Riemann have made significant contributions to the field of calculus. Fractional calculus is used to model many real-world problems, providing a robust framework for modeling systems with memory, long-range dependence, and complex dynamics [1]. Fractional calculus remains a dynamically active area of research, finding applications in various scientific and engineering disciplines, such as biology [2], bioengineering [3], and many more can be found in [4–6]. Real world problems based on the fractional integro-differential equations can be referred to the following literature [7, 8].

In this article, we discussed the following fractional order Volterra integro-differential equation (FOVIDE) [9]:

$$\begin{cases} \mathcal{D}_t^{\nu}\mathcal{Y}(t) + \mathcal{A}(t)\mathcal{Y}(t) + \lambda \int_0^t \mathcal{K}(t,s)\mathcal{Y}(s)ds = \mathcal{G}(t), & t \in [0,T], \\ \mathcal{Y}(0) = a, \end{cases} \tag{1.1}$$

where $\mathcal{D}_t^{\nu}$ represents the Caputo non-integer differential operator of order $\nu \in (0,1)$. The parameter λ denotes the physical quantity in particle motion. The real constant a denotes the initial condition and $T \in \mathbb{R}^+$. The function $\mathcal{A}(t) > 0$, $\mathcal{G}(t)$ are sufficiently smooth on $[0,T]$ and $\mathcal{K}(t,s) > 0$ on $[0,T] \times [0,T]$ represents the kernel function.

The existence and uniqueness of the solution of fractional order Volterra integro-differential equations (FOVIDEs) can be found in [4, 10]. P. Das et al. [11] derived the conditions for the existence and uniqueness of the solution based on maximum norm for weakly singular FOVIDE. Dong et al. [12] used Banach and Schaude fixed point technique for the existence and uniqueness of solutions of FOVIDE. The existence, uniqueness, and well-posedness for more general class of fractional order integro-differential equations is available in [13–16]. Numerous analytical and semi-analytical methods have their limitations and also to obtain the analytical solutions of FOVIDEs is not that much easy. In parallel, researchers have designed numerical techniques to discover approximations for the FOVIDEs. In [17–19], homotopy perturbation methods has been used to obtain the approximate solution for fractional order Volterra-Fredholm integro differential equations. Weijiang et al. [20] solved FOVIDE by using reproducing kernel method. M. Abbar et al. [21] presented optimal homotopy asymptotic method to obtain numerical solution. A. Pedas et al.[22] discussed the numerical solution of FOVIDEs by using smoothing transformations along with spline collocation technique. P. Yadav et al. [23] proposed operation matrix method which is based on Legendre wavelets and interpolating scaling function to solve FOVIDE. Here, we discuss some recent numerical approaches to solve FOVIDEs:

- Lizhu et al. [24] solved the nonlinear FOVIDEs by using second kind Chebyshev wavelet operational matrix method.
- M. H. Heydari et al. [25] obtained approximate solution of FOVIDE by using operational matrix of fractional derivative of Chebyshev wavelets.
- N. Rajagopal et al. [26] obtained numerical method based on Bernoulli wavelet approximation. Error estimation and convergence analysis of the proposed method has been established.
- Maurya et al. [27] proposed the Gram-Schmidt orthogonalization algorithm to approximate the solution using randomly distributed points and Gauss-Legendre roots as collocation node points.
- S. Santra et al. [28] used the classical L1 scheme with composite trapezoidal approximation to provide the numerical solution for FOVIDE and also discussed the error analysis of the proposed method.
- B. Ghosh et al. [9] proposed two finite difference schemes that uses the L1 and L1-2 discretization. Stability and convergence of the schemes have been established via maximum norm.

Based on our understanding from the literature survey, we observed that a method based on the API formula is not available for solving the proposed model (1.1). In this work, we aim to develop a method using the API formula to solve the model (1.1). The following points outline the main work of this paper:

- We have constructed two new schemes, Scheme-I and Scheme-II for the model (1.1). For Scheme-I, we approximated the Caputo derivative by the classical L1 formula and the Volterra part by the API method. Scheme-II is obtained by approximating the Caputo derivative by the L1-2 formula and the Volterra part by the API method. The appropriate algorithms are also provided to obtain Scheme-I and Scheme-II.
- The truncation error of the L1 formula, L1-2 formula, and API method are bounded by $Ch^{2-\nu}$, $Ch^{3-\nu}$ and $Ch^{\mathcal{M}+1}$, respectively. To obtain these bounds, the solution is required to be in $C^3[0,1]$. However, if one uses the moving mesh methods [29–33], the required smoothness can be significantly reduced to $C^1[0,1]$ or piecewise smoothness.
- Stability and convergence of the proposed schemes are analyzed and measured in terms of maximum norm. It is proven that Scheme-I and Scheme-II have achieved $\mathcal{O}\left(h^{2-\nu}\right)$ and $\mathcal{O}\left(h^{3-\nu}\right)$ order of convergence, respectively.
- Numerical experiments are performed in which three test problems are solved by the proposed schemes. Numerical results obtained by the presented schemes for the first and the third test problems are compared with each other and are also compared with the existing method[9]. The second test problem is taken as a FOVIDE with a weakly singular kernel. The numerical stability of the proposed schemes has also been analyzed, and it found that both schemes are numerically stable.

The rest of the paper is organized as follows: In Section 2, some definitions, background information, applicability, and properties of the API method are discussed. In Section 3, discretized schemes for solving the FOVIDE are constructed. Error analysis by which convergence and stability of the proposed schemes is established in Section 4. In Section 5, numerical experiments are carried out to check the efficiency and accuracy of the presented schemes. In Section 6, the numerical stability of the proposed schemes has been established. Finally, some concluding remarks are given in Section 7.

1.1 | Notation

In this article, C denotes a generic positive constant in several inequalities with different values at different occurrences. $C^n(\Omega)$ represents the space of n-th order real valued continuously differentiable functions on Ω, we use $C(\Omega)$ for $C^0(\Omega)$. Set $\psi_i = \psi(t_i)$ for any function ψ defined on a domain Ω. Discrete maximum norm is defined by $\|\psi\|_\infty = \max_i|\psi(t_i)|$. $\mathbb{R}$ signifies set of real numbers while $\mathbb{R}^+$ represents the set of positive real numbers. $\mathbb{N}$ denotes the set of positive integers.

2 | BASIC DEFINITIONS AND PRELIMINARIES

Definition 2.1. Riemann-Liouville fractional integral [34]: If $\mathcal{Y}(t) \in C[a, b]$, $t \in \mathbb{R}^+$, and $\nu \in \mathbb{R}^+$ then

$$\mathcal{I}^\nu \mathcal{Y}(t) = \frac{1}{\Gamma(\nu)} \int_a^t \frac{\mathcal{Y}(s)}{(t-s)^{1-\nu}} ds,$$

is called Riemann-Liouville fractional integral of order ν.

Definition 2.2. Caputo fractional derivative [35]: The Caputo non-integer derivative with order $\nu \in \mathbb{R}^+$ of function $\mathcal{Y}(t) \in AC^n[a, b] := \{\mathcal{Y} : [\mathrm{a}, \mathrm{b}] \to \mathbb{R} : \mathrm{D}^{\mathrm{n}-1}\mathcal{Y}(\mathrm{t}) \in \mathrm{AC}\,[\mathrm{a}, \mathrm{b}]\}$ is defined by

$$\mathcal{D}_t^\nu \mathcal{Y}(t) = \begin{cases} \frac{1}{\Gamma(n-\nu)} \int_a^t \frac{\mathcal{Y}^{(n)}(s)}{(t-s)^{\nu-n+1}} ds, & n-1 < \nu < n, \\ \mathcal{Y}^{(n)}(t), & \nu = n \in \mathbb{N}. \end{cases}$$

Here, $\Gamma(\cdot)$ is the Gamma function, $D^n = \left(\frac{d}{dt}\right)^n$, and $AC[a, b]$ represents the space of all absolutely continuous functions on [a, b].

2.1 | Approximate product integration

In this technique, integrals of the products of two functions $f(t)$ and $\phi(t)$ are expressed as [36]

$$\int_a^b f(t)\phi(t)dt = \sum_{r=1}^n \delta_r f(t_r) + \mathcal{R}, \tag{2.1}$$

where $t_1 < t_2 < \ldots < t_n$ are n abscissa, $\delta_1, \delta_2, \ldots, \delta_n$ are associated weights, and $\mathcal{R}$ is correction term. Let

$$f(t) = \sum_{s=0}^{m-1} a_s F_s(t) + C(t), \tag{2.2}$$

be the expansion of $f(t)$ as the linear combination of m linearly independent functions $F_0(t), F_1(t), \cdots, F_{m-1}(t)$ in some range $\chi_1 \le a \le b \le \chi_2$, where $a_0, a_1, \cdots, a_{m-1}$ are constants and $C(t)$ is remainder term which can be determined.

If each abscissa lies within the range $\chi_1 \le t \le \chi_2$ then the expression for $f(t)$ and $f(t_r)$ given by (2.2) can be substituted in (2.1). It follows that

$$\mathcal{R} = \int_a^b C(t)\phi(t)dt - \sum_{r=1}^n \delta_r C(t_r), \tag{2.3}$$

provided that

$$\int_a^b F_s(t)\phi(t)dt = \sum_{r=1}^{n} \delta_r F_s(t_r), \quad s = 0, \cdots, m-1. \tag{2.4}$$

This gives us m equations for n weights and n ordinates. When $m = n$ and all the abscissae are known, the weights δ_r can be calculated from (2.4). Two points are important in application:

- The abscissae need not lie in the range of the integration. Abscissae may lie within the range where the expansion of $f(t)$ is valid.
- $\phi(t)$ can have weak singularity within the range of integration and may be discontinuous, and it is required that for each value of s, the integral $\int_a^b F_s(t)\phi(t)dt$ exists.

Let

$$\eta_s = \int_a^b F_s(t)\phi(t)dt, \; s = 0, \cdots, m-1.$$

η_s is known as the generalized moment of the moment function $\phi(t)$ of order s . Let F be the mxn matrix whose i, j^{th} element is $F_{i,j} = F_{i-1}(t_j)$, δ be the column vector of the n weights $\delta_1, \delta_2, \cdots, \delta_n$, and η be the column vector of the m moments $\eta_0, \eta_1, \ldots, \eta_{m-1}$, then Equation (2.4) can be written as

$$F\delta = \eta. \tag{2.5}$$

Different expansions (2.2) of $f(t)$ can be taken, for example, Beard [37] used Maclaurin expansion of $f(t)$. A. Young [36] considered expansion of $f(t)$ other than Maclaurin series; however, the focus is mostly on the Newton-Cotes type formula obtained from the Taylor series expansion of $f(t)$.

Provided the moments of the kernel function exist, this technique can be applied to obtain the numerical solutions of singular as well as weakly singular integral equations of both Fredholm and Volterra type in which the formulas for numerical integration are derived from the kernel of the integral equations [38].

3 | FORMULATION OF THE DISCRETE PROBLEM

In this section, discretized problems are obtained by approximating (1.1) using finite difference formulas and the approximate product integration method. We consider the uniform mesh, $0 = t_0 < t_1 < \ldots < t_{\mathscr{M}} = T$ with step size $h = t_{j+1} - t_j$, $0 \le j \le \mathscr{M} - 1$, where $\mathscr{M} \in \mathbb{N}$.

3.1 | Scheme-I: Discretization by using L1 approximation and API method

The Caputo non-integer derivative $\mathcal{D}_t^{\nu}\mathcal{Y}(t)$ at t_j can be written as

$$\mathcal{D}_t^{\nu}\mathcal{Y}(t_j) = \frac{1}{\Gamma(1-\nu)} \sum_{q=0}^{j-1} \int_{t_q}^{t_{q+1}} \frac{\mathcal{Y}'(s)}{(t_j - s)^{\nu}} ds,$$

which is approximated by classical L1 scheme [39] as

$$L_1 p\mathcal{D}^{\nu}\mathcal{Y}(t_j) = \frac{1}{\Gamma(1-\nu)} \sum_{q=0}^{j-1} \frac{\mathcal{Y}(t_{q+1}) - \mathcal{Y}(t_q)}{h} \int_{t_q}^{t_{q+1}} \frac{ds}{(t_j - s)^{\nu}} = \frac{h^{-\nu}}{\Gamma(2-\nu)} \sum_{q=0}^{j-1} [\mathcal{Y}(t_{q+1}) - \mathcal{Y}(t_q)]\sigma_{j-q} + \zeta_j^{(L1)}, \tag{3.1}$$

where $\zeta_j^{(L1)} = (\mathcal{D}_t^{\nu} - L_1 p\mathcal{D}^{\nu})\mathcal{Y}(t_j)$, and

$$\sigma_r = r^{1-\nu} - (r-1)^{1-\nu}, \text{ for } \; r = 1, \cdots, \mathscr{M}. \tag{3.2}$$

For the Volterra part in (1.1), we use the approximate product integration method [36] using formula of the form:

$$\int_{t_0}^{t_j} \mathcal{K}(t_j,s)\mathcal{Y}(s)ds = \sum_{i=0}^{\mathcal{M}} \alpha_{i,j}\mathcal{Y}(t_i) + \zeta_j^{(P)}, \quad j = 0,\cdots,\mathcal{M}, \tag{3.3}$$

where $\alpha_{i,j}$ are the weights associated with $t_0, t_1, \cdots, t_{\mathcal{M}}$ and $\zeta_j^{(P)}$ is correction term. Take the Taylor series expansion of $\mathcal{Y}(t)$ at $t = t_{\mathcal{M}}$ using end point formula, we have

$$\mathcal{Y}(t) = \sum_{i=0}^{\mathcal{M}} \frac{F_i(t)}{i!}\mathcal{Y}^{(i)}(t_{\mathcal{M}}) + R(t),$$

where $F_i(t) = (t - t_{\mathcal{M}})^i$, and the remainder term is given by $R(t) = \frac{F_{\mathcal{M}+1}(t)}{(\mathcal{M}+1)!}\mathcal{Y}^{(\mathcal{M}+1)}(\xi)$, $0 < \xi < L$.

Let A and W be $(\mathcal{M}+1)\times(\mathcal{M}+1)$ weight and moment matrices with i,j-th entry $\alpha_{i,j}$ and $c_{i,j}$, respectively, where

$$c_{i,j} = \int_{t_0}^{t_j} F_i(s)\mathcal{K}(t_j,s)ds, \quad j = 0,\cdots,\mathcal{M}. \tag{3.4}$$

Let χ be the $(\mathcal{M}+1)\times(\mathcal{M}+1)$ invertible matrix for the points $t_0, t_1, \cdots, t_M$ with entries

$$\chi_{i,j} = F_i(t_j).$$

Weights in (3.3) are given by

$$\chi A = W. \tag{3.5}$$

Also, the correction term $\zeta_j^{(P)}$ in (3.3) is given by

$$\zeta_j^{(P)} = \int_{t_0}^{t_j} \mathcal{K}(t_j,s)R(t)ds - \sum_{i=0}^{\mathcal{M}} \alpha_{i,j}R(t_i). \tag{3.6}$$

Making the use of (3.1) and (3.3), (1.1) becomes

$$\begin{cases} L_1 p\mathcal{D}^\nu \mathcal{Y}(t_j) + \mathcal{A}(t_j)\mathcal{Y}(t_j) + \lambda \sum\limits_{i=0}^{\mathcal{M}} \alpha_{i,j}\mathcal{Y}(t_i) = \mathcal{G}(t_j) + \zeta_j^{(1)}, \quad j = 1,\cdots,\mathcal{M}, \\ \mathcal{Y}(t_0) = a, \end{cases} \tag{3.7}$$

where

$$\zeta_j^{(1)} = \zeta_j^{(L1)} + \zeta_j^{(P)}. \tag{3.8}$$

The discrete problem corresponding to (1.1) after omitting the remainder term $\zeta_j^{(1)}$ is given by

$$\begin{cases} L_1 p\mathcal{D}^\nu \hat{\mathcal{Y}}_j + \mathcal{A}_j\hat{\mathcal{Y}}_j + \lambda \sum\limits_{i=0}^{\mathcal{M}} \alpha_{i,j}\hat{\mathcal{Y}}_i = \mathcal{G}_j, \quad j = 1,\cdots,\mathcal{M}, \\ \hat{\mathcal{Y}}_0 = a, \end{cases} \tag{3.9}$$

where approximation of the solution $\mathcal{Y}$ at the grid point t_j is denoted by $\hat{\mathcal{Y}}_j$, then (3.9) can be re-written as

$$\begin{cases} \mu \sum\limits_{q=0}^{j-1} [\mathcal{Y}(t_{q+1}) - \mathcal{Y}(t_q)]\sigma_{j-q} + \mathcal{A}_j\hat{\mathcal{Y}}_j + \lambda \sum\limits_{i=0}^{\mathcal{M}} \alpha_{i,j}\hat{\mathcal{Y}}_i = \mathcal{G}_j, \quad j = 1,\cdots,\mathcal{M}, \\ \hat{\mathcal{Y}}_0 = a, \end{cases} \tag{3.10}$$

where $\mu = \frac{h^{-\nu}}{\Gamma(2-\nu)}$. For $j = 1, 2, , \dots , \mathcal{M}$, we get the following system of equations:

$$\begin{aligned}
&(\mu\sigma_1 + \mathcal{A}_1 + \lambda\alpha_{1,1})\hat{\mathcal{Y}}_1 + \lambda\alpha_{2,1}\hat{\mathcal{Y}}_2 + \cdots\cdots + \lambda\alpha_{\mathcal{M},1}\hat{\mathcal{Y}}_{\mathcal{M}} = \mathcal{G}_1 - (-\mu\sigma_1 + \lambda\alpha_{0,1})\hat{\mathcal{Y}}_0,\\
&(\mu(\sigma_2 - \sigma_1) + \lambda\alpha_{1,2})\hat{\mathcal{Y}}_1 + (\mu\sigma_1 + \mathcal{A}_2 + \lambda\alpha_{2,2})\hat{\mathcal{Y}}_2 + \cdots + \lambda\alpha_{\mathcal{M},2}\hat{\mathcal{Y}}_{\mathcal{M}} = \mathcal{G}_2 - (-\mu\sigma_2 + \lambda\alpha_{0,2})\hat{\mathcal{Y}}_0,\\
&\qquad\vdots \qquad + \qquad \vdots \qquad + \cdots + \qquad \vdots = \qquad \vdots\\
&(\mu(\sigma_{\mathcal{M}} - \sigma_{\mathcal{M}-1}) + \lambda\alpha_{1,\mathcal{M}})\hat{\mathcal{Y}}_1 + (\mu(\sigma_{\mathcal{M}-1} - \sigma_{\mathcal{M}-2}) + \lambda\alpha_{2,\mathcal{M}})\hat{\mathcal{Y}}_2 + \cdots\\
&\qquad + (\mu\sigma_1 + \mathcal{A}_{\mathcal{M}} + \lambda\alpha_{\mathcal{M},\mathcal{M}})\hat{\mathcal{Y}}_{\mathcal{M}} = \mathcal{G}_{\mathcal{M}} - (-\mu\sigma_{\mathcal{M}} + \lambda\alpha_{0,\mathcal{M}})\hat{\mathcal{Y}}_0.
\end{aligned} \tag{3.11}$$

The matrix form of the above system (3.11) is given by

$$\mathcal{P}\hat{\mathcal{Y}} = \mathcal{Q}, \tag{3.12}$$

where $\hat{\mathcal{Y}} = [\hat{\mathcal{Y}}_1, \hat{\mathcal{Y}}_2, \cdots, \hat{\mathcal{Y}}_{\mathcal{M}}]^T$,

$$\mathcal{P} = \begin{bmatrix} \mu\sigma_1 + \mathcal{A}_1 + \lambda\alpha_{1,1} & \lambda\alpha_{2,1} & \cdots & \lambda\alpha_{\mathcal{M},1}\\ \mu(\sigma_2 - \sigma_1) + \lambda\alpha_{1,2} & \mu\sigma_1 + \mathcal{A}_2 + \lambda\alpha_{2,2} & \cdots & \lambda\alpha_{\mathcal{M},2}\\ \vdots & \vdots & \vdots & \vdots\\ \mu(\sigma_{\mathcal{M}} - \sigma_{\mathcal{M}-1}) + \lambda\alpha_{1,\mathcal{M}} & \mu(\sigma_{\mathcal{M}-1} - \sigma_{\mathcal{M}-2}) + \lambda\alpha_{2,\mathcal{M}} & \dots & \mu\sigma_1 + \mathcal{A}_{\mathcal{M}} + \lambda\alpha_{\mathcal{M},\mathcal{M}} \end{bmatrix},$$

$$\mathcal{Q} = \begin{bmatrix} \mathcal{G}_1 - (-\mu\sigma_1 + \lambda\alpha_{0,1})\hat{\mathcal{Y}}_0\\ \mathcal{G}_2 - (-\mu\sigma_2 + \lambda\alpha_{0,2})\hat{\mathcal{Y}}_0\\ \vdots\\ \mathcal{G}_{\mathcal{M}} - (-\mu\sigma_{\mathcal{M}} + \lambda\alpha_{0,\mathcal{M}})\hat{\mathcal{Y}}_0 \end{bmatrix}.$$

Algorithm 1: To find the approximate solution of the model problem (1.1) using Scheme-I.

Input: The constant $\nu \in (0, 1)$, $T \in \mathbb{R}^+, \mathcal{M} \in \mathbb{Z}^+$, $\mathcal{A} : [0, L] \to \mathbb{R}^+$, $\mathcal{K} : [0, T] \times [0, T] \to \mathbb{R}^+, \mathcal{G}$ is sufficiently smooth on [0,T].

Output: The numerical solutions $\mathcal{Y}_j$.

for *Numerical solution of FOVIDEs* (1.1) *by present Scheme-I based on L1 approximation and API method on uniform grid.* **do**

Step-1.1 Split the interval $[0, T]$ as mentioned in the beginning of the Section 3.

Step-1.2 Approximate the Caputo non-integer derivative as $L_1 p\mathcal{D}^\nu\mathcal{Y}(t_j) \approx \frac{h^{-\nu}}{\Gamma(2-\nu)} \sum_{q-0}^{j-1} [\mathcal{Y}(t_{q+1}) - \mathcal{Y}(t_q)]\sigma_{j-q}$, given in Equation (3.1).

Step-1.3 Volterra part in (1.1) is approximated by using API method as $\int_{t_0}^{t_j} \mathcal{K}(t_j, s)\mathcal{Y}(s)ds \approx \sum_{i=0}^{\mathcal{M}} \alpha_{i,j}\mathcal{Y}(t_i)$, given in Equation (3.3).

Step-1.4 Put the values of (3.1) and (3.3) in (1.1) and neglect the remainder term to get the discrete scheme given by Equation (3.9).

Step-1.5 Discrete scheme given by Equation (3.9) is applied to get approximate solution $\hat{\mathcal{Y}}_j$.

.

end

3.2 | Scheme-II: Discretization by using L1-2 approximation and API method

Let, $t_{q+\frac{1}{2}} = \frac{t_{q+1}+t_q}{2}$, for $q \geq 0$. The difference quotient operators are
$\Delta_t\mathcal{Y}_{q-\frac{1}{2}} = \frac{\mathcal{Y}(t_q)-\mathcal{Y}(t_{q-1})}{h}$, $\Delta_t\mathcal{Y}_{q+\frac{1}{2}} = \frac{\mathcal{Y}(t_{q+1})-\mathcal{Y}(t_q)}{h}$, and $\Delta_t^2\mathcal{Y}_q = \frac{\Delta_t\mathcal{Y}_{q+\frac{1}{2}}-\Delta_t\mathcal{Y}_{q-\frac{1}{2}}}{h}$.
The Caputo non-integer derivative $\mathcal{D}_t^\nu\mathcal{Y}(t)$ at t_j can be written as

$$\mathcal{D}_t^\nu\mathcal{Y}(t_j) = \frac{1}{\Gamma(1-\nu)} \left[\int_{t_0}^{t_1} \frac{\mathcal{Y}'(s)}{(t_j - s)^\nu} ds + \sum_{q=1}^{j-1} \int_{t_q}^{t_{q+1}} \frac{\mathcal{Y}'(s)}{(t_j - s)^\nu} ds \right].$$

Its approximation is given by

$$L1\text{-}2_p\mathcal{D}^\nu\mathcal{Y}(t_j) = \frac{1}{\Gamma(1-\nu)}\left[\int_{t_0}^{t_1}\frac{(\Pi_{1,1}\mathcal{Y}(s))'}{(t_j-s)^\nu}ds + \sum_{q=1}^{j-1}\int_{t_q}^{t_{q+1}}\frac{(\Pi_{2,q}\mathcal{Y}(s))'}{(t_j-s)^\nu}ds\right]. \tag{3.13}$$

Here, $\Pi_{1,1}\mathcal{Y}(t)$ represents the linear interpolation function of $\mathcal{Y}(t)$ on $[t_{q-1}, t_q]$, that is,

$$\Pi_{1,1}\mathcal{Y}(t) = \frac{t_q - t}{h}\mathcal{Y}(t_{q-1}) + \frac{t - t_{q-1}}{h}\mathcal{Y}(t_q), \tag{3.14}$$

and for $q \geq 1$, $\Pi_{2,q}\mathcal{Y}(t)$ represents the quadratic interpolation function of $\mathcal{Y}(t)$ on $[t_q, t_{q+1}]$, that is,

$$\Pi_{2,q}\mathcal{Y}(t) = \frac{(t-t_q)(t-t_{q+1})}{2h^2}\mathcal{Y}(t_{q-1}) + \frac{(t-t_{q-1})(t_{q+1}-t)}{2h^2}\mathcal{Y}(t_q) + \frac{(t-t_q)(t-t_{q-1})}{2h^2}\mathcal{Y}(t_{q+1}). \tag{3.15}$$

Put (3.14) and (3.15) in (3.13), we have the $L1$-2 scheme [40] as

$$\begin{aligned}
L1\text{-}2_p\mathcal{D}^\nu\mathcal{Y}(t_j) &= \frac{1}{\Gamma(1-\nu)}\left[\Delta_t\mathcal{Y}_{\frac{1}{2}}\int_{t_0}^{t_1}\frac{ds}{(t_j-s)^\nu} + \sum_{q=1}^{j-1}\int_{t_q}^{t_{q+1}}\frac{\Delta_t\mathcal{Y}_{q+\frac{1}{2}} + (s-t_{q+\frac{1}{2}})\Delta_t^2\mathcal{Y}_q}{(t_j-s)^\nu}ds\right] \\
&= \frac{1}{\Gamma(1-\nu)}\left[\sum_{q=0}^{j-1}\Delta_t\mathcal{Y}_{q+\frac{1}{2}}\int_{t_q}^{t_{q+1}}\frac{ds}{(t_j-s)^\nu} + \sum_{q=1}^{j-1}\Delta_t^2\mathcal{Y}_q\int_{t_q}^{t_{q+1}}\frac{s-t_{q+\frac{1}{2}}}{(t_j-s)^\nu}ds\right] \\
&= \frac{h^{-\nu}}{\Gamma(2-\nu)}\left[\sum_{q=0}^{j-1}[\mathcal{Y}(t_{q+1})-\mathcal{Y}(t_q)]\sigma_{j-q} + \sum_{q=1}^{j-1}[\mathcal{Y}(t_{q+1})-2\mathcal{Y}(t_q)+\mathcal{Y}(t_{q-1})]\sigma^*_{j-q}\right] + \zeta_j^{(L1\text{-}2)} \\
&= \frac{h^{-\nu}}{\Gamma(2-\nu)}\sum_{q=0}^{j-1}[\mathcal{Y}(t_{q+1})-\mathcal{Y}(t_q)]\rho_{j-q} + \zeta_j^{(L1\text{-}2)}.
\end{aligned} \tag{3.16}$$

Here, $\zeta_j^{(L1\text{-}2)} = (\mathcal{D}_t^\nu - L1\text{-}2_p\mathcal{D}^\nu)\mathcal{Y}(t_j)$ and ρ_r are defined below. For $j=1$, $\rho_1 = 1$, and for $j \geq 2$,

$$\rho_r = \begin{cases} \sigma_1 + \sigma_1^*, & \text{if } r = 1, \\ \sigma_r + \sigma_r^* - \sigma_{r-1}^*, & \text{if } 2 \leq r \leq j-1, \\ \sigma_r + \sigma_r^*, & \text{if } r = j, \end{cases} \tag{3.17}$$

where σ_r is already defined in (3.2) and σ_r^* are defined as

$$\sigma_r^* = \frac{1}{(2-\nu)}[r^{(2-\nu)} - (r-1)^{2-\nu}] - \frac{1}{2}[r^{(1-\nu)} + (r-1)^{(1-\nu)}], \quad \text{for } r = 1, \cdots, \mathscr{M}. \tag{3.18}$$

After substituting the values of Equations (3.3) and (3.16) in the model (1.1), we get

$$\begin{cases} L1\text{-}2_p\mathcal{D}^\nu\mathcal{Y}(t_j) + \mathcal{A}(t_j)\mathcal{Y}(t_j) + \lambda\sum_{i=0}^{\mathscr{M}}\alpha_{i,j}\mathcal{Y}(t_i) = \mathcal{G}(t_j) + \zeta_j^{(2)}, \quad j = 1, \cdots, \mathscr{M}, \\ \mathcal{Y}(t_0) = a, \end{cases} \tag{3.19}$$

where

$$\zeta_j^{(2)} = \zeta_j^{(L1\text{-}2)} + \zeta_j^{(P)}. \tag{3.20}$$

The discrete problem corresponding to (1.1) after omitting the remainder term $\zeta_j^{(2)}$ is given by

$$\begin{cases} L1\text{-}2_p\mathcal{D}^\nu\tilde{\mathcal{Y}}_i + \mathcal{A}_j\tilde{\mathcal{Y}}_j + \lambda\sum_{i=0}^{\mathscr{M}}\alpha_{i,j}\tilde{\mathcal{Y}}_i = \mathcal{G}_j, \quad j = 1, \cdots, \mathscr{M}, \\ \tilde{\mathcal{Y}}_0 = a, \end{cases} \tag{3.21}$$

where the approximation of the solution $\mathcal{Y}$ at the grid point t_j is denoted by $\tilde{\mathcal{Y}}_j$, $\mathcal{A}(t_j)$ is denoted by $\mathcal{A}_j$ and $\mathcal{G}(t_j)$ is denoted by $\mathcal{G}_j$. The above scheme (3.21) can be re-written as

$$\begin{cases} \mu \sum_{q=0}^{j-1} \left[\tilde{\mathcal{Y}}(t_{q+1}) - \tilde{\mathcal{Y}}(t_q)\right] \rho_{j-q} + \mathcal{A}_j \tilde{\mathcal{Y}}_j + \lambda \sum_{i=0}^{\mathcal{M}} \alpha_{i,j} \tilde{\mathcal{Y}}_i = \mathcal{G}_j, \quad j = 1, \cdots, \mathcal{M}, \\ \tilde{\mathcal{Y}}_0 = a, \end{cases} \tag{3.22}$$

where $\mu = \frac{h^{-\nu}}{\Gamma(2-\nu)}$. For $j = 1, \dots, \mathcal{M}$, the above scheme (3.22) can be written as the linear system of the equations as follows:

$$\begin{aligned}
&(\mu\rho_1 + \mathcal{A}_1 + \lambda\alpha_{1,1})\tilde{\mathcal{Y}}_1 + \lambda\alpha_{2,1}\tilde{\mathcal{Y}}_2 + \cdots\cdots\cdots + \lambda\alpha_{\mathcal{M},1}\tilde{\mathcal{Y}}_{\mathcal{M}} = \mathcal{G}_1 - (-\mu\rho_1 + \lambda\alpha_{0,1})\tilde{\mathcal{Y}}_0,\\
&(\mu(\rho_2 - \rho_1) + \lambda\alpha_{1,2})\tilde{\mathcal{Y}}_1 + (\mu\rho_1 + \mathcal{A}_2 + \lambda\alpha_{2,2})\tilde{\mathcal{Y}}_2 + \cdots + \lambda\alpha_{\mathcal{M},2}\tilde{\mathcal{Y}}_{\mathcal{M}} = \mathcal{G}_2 - (-\mu\rho_2 + \lambda\alpha_{0,2})\tilde{\mathcal{Y}}_0,\\
&\quad \vdots \quad + \quad \vdots \quad + \cdots + \quad \vdots = \quad \vdots\\
&(\mu(\rho_{\mathcal{M}} - \rho_{\mathcal{M}-1}) + \lambda\alpha_{1,\mathcal{M}})\tilde{\mathcal{Y}}_1 + (\mu(\rho_{\mathcal{M}-1} - \rho_{\mathcal{M}-2}) + \lambda\alpha_{2,\mathcal{M}})\tilde{\mathcal{Y}}_2 + \cdots\\
&\qquad\qquad + (\mu\rho_1 + \mathcal{A}_{\mathcal{M}} + \lambda\alpha_{\mathcal{M},\mathcal{M}})\tilde{\mathcal{Y}}_{\mathcal{M}} = \mathcal{G}_{\mathcal{M}} - (-\mu\rho_{\mathcal{M}} + \lambda\alpha_{0,\mathcal{M}})\tilde{\mathcal{Y}}_0.
\end{aligned}$$

The matrix form of the above system is given by

$$Y\tilde{\mathcal{Y}} = Z, \tag{3.23}$$

where $\tilde{\mathcal{Y}} = [\tilde{\mathcal{Y}}_1, \tilde{\mathcal{Y}}_2, \dots, \tilde{\mathcal{Y}}_{\mathcal{M}}]^T$,

$$Y = \begin{bmatrix} \mu\rho_1 + \mathcal{A}_1 + \lambda\alpha_{1,1} & \lambda\alpha_{2,1} & \dots & \lambda\alpha_{\mathcal{M},1} \\ \mu(\rho_2 - \rho_1) + \lambda\alpha_{1,2} & \mu\rho_1 + \mathcal{A}_2 + \lambda\alpha_{2,2} & \dots & \lambda\alpha_{\mathcal{M},2} \\ \vdots & \vdots & \vdots & \vdots \\ \mu(\rho_{\mathcal{M}} - \rho_{\mathcal{M}-1}) + \lambda\alpha_{1,\mathcal{M}} & \mu(\rho_{\mathcal{M}-1} - \rho_{\mathcal{M}-2}) + \lambda\alpha_{2,\mathcal{M}} & \dots & \mu\rho_1 + \mathcal{A}_{\mathcal{M}} + \lambda\alpha_{\mathcal{M},\mathcal{M}} \end{bmatrix},$$

$$Z = \begin{bmatrix} \mathcal{G}_1 - (-\mu\rho_1 + \lambda\alpha_{0,1})\tilde{\mathcal{Y}}_0 \\ \mathcal{G}_2 - (-\mu\rho_2 + \lambda\alpha_{0,2})\tilde{\mathcal{Y}}_0 \\ \vdots \\ \mathcal{G}_{\mathcal{M}} - (-\mu\rho_{\mathcal{M}} + \lambda\alpha_{0,\mathcal{M}})\tilde{\mathcal{Y}}_0 \end{bmatrix}.$$

Algorithm 2: To find the approximate solution of the model problem (1.1) using Scheme-II.

Input: The constants $\nu \in (0, 1)$, $T \in \mathbb{R}^+$, $\mathcal{M} \in \mathbb{Z}^+$, $\mathcal{A} : [0, T] \to \mathbb{R}^+$, $\mathcal{K} : [0, T] \times [0, T] \to \mathbb{R}^+$, $\mathcal{G}$ is sufficiently smooth on [0,T].

Output: The numerical solution $\tilde{\mathcal{Y}}_j$.

for *Numerical solution of FOVIDEs* (1.1) *by present Scheme-II based on L1-2 approximation and API method on uniform grid.* **do**

Step-1.1 Split the interval $[0, T]$ as mentioned in the beginning of the Section 3.

Step-1.2 Approximate the Caputo non-integer derivative as $L1\text{-}2_p\mathcal{D}^\nu\mathcal{Y}(t_j) \approx \frac{h^{-\nu}}{\Gamma(1-\nu)} \sum_{q=0}^{j-1} [\mathcal{Y}(t_{q+1}) - \mathcal{Y}(t_q)]\rho_{j-q}$, given in Equation (3.16).

Step-1.3 Volterra part in (1.1) is approximated by using API method as $\int_{t_0}^{t_j} \mathcal{K}(t_j, s)\mathcal{Y}(s)ds \approx \sum_{i=0}^{\mathcal{M}} \alpha_{i,j}\mathcal{Y}(t_i)$, given in Equation (3.3).

Step-1.4 Put the values of (3.16) and (3.3) in (1.1) and neglecting the remainder term to get the discrete scheme given by Equation (3.21).

Step-1.5 Discrete scheme given by Equation (3.21) is applied to get approximate solution $\tilde{\mathcal{Y}}_j$.

.

end

4 | STABILITY AND CONVERGENCE

In this section, we established the stability and convergence of the proposed Scheme-I and Scheme-II with respect to the maximum norm . Firstly, for Scheme-I, we provide some lemmas and bounds for the remainder terms associated with the approximation of Caputo non-integer derivative by the $L1$ formula and with the approximation of the Volterra part by the API method. The global error is computed by using these results to establish the convergence of Scheme-I. The same procedure is followed to establish the stability and convergence for the Scheme-II.

4.1 | Stability and convergence analysis for Scheme-I

Although we get the asymptotic of solution at the starting time, we have to consider an ideal case, that is, in [0, T] since the analysis of the numerical scheme based on API method and L1 and L1-2 formula is really difficult to investigate. For ideal compatibility conditions, the interested reader can refer to the following literature [41–44].

Lemma 4.1 ([9]). *For any mesh function $\{\hat{\mathcal{Y}}_j\}_{j=0}^{\mathcal{M}}$ with $\mathcal{Y}_0 = 0$, we have*

$$\left|\hat{\mathcal{Y}}_j\right| \leq \max_{1\leq r\leq \mathcal{M}} \left\{ \frac{h^{\nu}\Gamma(2-\nu)}{\sigma_r} L_1 p\mathcal{D}^{\nu}\left|\hat{\mathcal{Y}}_r\right| \right\}, \quad j = 1, \cdots, \mathcal{M}.$$

Lemma 4.2 ([9]). *Let $\mathcal{Y}(t) \in C^3[0,T]$ be the analytical solution of (1.1), then the remainder term of $L1$ approximation (3.1) satisfies*

$$\left|\zeta_j^{L1}\right| \leq Ch^{2-\nu}, \quad j = 1, \cdots, \mathcal{M}.$$

Lemma 4.3. *Assume that $\mathcal{Y}(t) \in C^3[0,T] \cup C^{\mathcal{M}+1}[0,T]$, where $\mathcal{M} \in \mathbb{N}$, then the correction term $\zeta_j^{(P)}$ of the API method (3.3) satisfies the following inequality:*

$$\left|\zeta_j^{(P)}\right| < Ch^{\mathcal{M}+1}, \quad for\ j = 1, \cdots, \mathcal{M}.$$

Proof. Since $\mathcal{Y}(t) \in C^{\mathcal{M}+1}[0,T]$, there exists constant C_1 such that

$$|\mathcal{Y}^i(t)| \leq C_1 \quad for\ i = 0, \cdots, \mathcal{M}+1.$$

Now, we have

$$\begin{aligned}
\left|\zeta_j^{(P)}\right| &= \left| \int_{t_0}^{t_j} \mathcal{K}(t_j,s)R(t)ds - \sum_{i=0}^{\mathcal{M}} \alpha_{i,j} R(t_i) \right| \\
&= \left| \int_{t_0}^{t_j} \frac{(s-t_{\mathcal{M}})^{\mathcal{M}+1}}{(\mathcal{M}+1)!} \mathcal{Y}^{\mathcal{M}+1}(\xi)\mathcal{K}(t_j,s)ds - \sum_{i=0}^{\mathcal{M}} \alpha_{i,j} \frac{(t_i-t_{\mathcal{M}})^{\mathcal{M}+1}}{(\mathcal{M}+1)!} \mathcal{Y}^{\mathcal{M}+1}(\xi) \right| \\
&= \left| \frac{h^{\mathcal{M}+1}}{(\mathcal{M}+1)!} \mathcal{Y}^{\mathcal{M}+1}(\xi) \right| \left| \int_{t_0}^{t_j} \frac{(s-t_{\mathcal{M}})^{\mathcal{M}+1}}{h^{\mathcal{M}+1}} \mathcal{K}(t_j,s)ds - \sum_{i=0}^{\mathcal{M}} \alpha_{i,j} \frac{(t_i-t_{\mathcal{M}})^{\mathcal{M}+1}}{h^{\mathcal{M}+1}} \right| \\
&\leq \frac{h^{\mathcal{M}+1}}{(\mathcal{M}+1)!} C_1 C_2 \\
&< Ch^{\mathcal{M}+1},
\end{aligned}$$

where $C_2 = \max_{0\leq j\leq \mathcal{M}} \left| \int_{t_0}^{t_j} \frac{(s-t_{\mathcal{M}})^{\mathcal{M}+1}}{h^{\mathcal{M}+1}} \mathcal{K}(t_j,s)ds - \sum_{i=0}^{\mathcal{M}} \alpha_{i,j} \frac{(t_i-t_{\mathcal{M}})^{\mathcal{M}+1}}{h^{\mathcal{M}+1}} \right|$, which completes the proof. ◻

Let $\hat{m}_j = |\mathcal{Y}(t_j) - \hat{\mathcal{Y}}_j|$ for $j = 1, \cdots, \mathcal{M}$, denote the absolute error at t_j. Using (3.7) and (3.9), we obtain following difference equations:

$$\begin{cases} L_1 p\mathcal{D}^{\nu}\hat{m}_j + \mathcal{A}_j\hat{m}_j + \lambda \sum_{i=0}^{\mathcal{M}} \alpha_{i,j}\hat{m}_i = \zeta_j^{(1)}, \ \text{for}\ j = 1, \cdots, \mathcal{M}, \\ \hat{m}_0 = 0. \end{cases} \tag{4.1}$$

Theorem 4.1. *For the difference Equation (4.1), solution satisfies the following inequality:*

$$\|\hat{E}\|_\infty \leq T^\nu \Gamma(1-\nu)\left\|\zeta^{(1)}\right\|_\infty,$$

where $\hat{E} = (\hat{m}_0, \hat{m}_1, \ldots, \hat{m}_{\mathscr{M}})'$, *and* $\zeta^{(1)} = (\zeta_0^{(1)}, \zeta_1^{(1)}, \ldots, \zeta_{\mathscr{M}}^{(1)})'$.

Proof. Using (3.1) without correction term in the difference Equation (4.1) and then multiplying it by $\hat{m}_j$, it follows that

$$\begin{aligned}\left|\frac{h^{-\nu}}{\Gamma(2-\nu)}\hat{m}_j^2 + \mathcal{A}_j\hat{m}_j^2 + \lambda\sum_{i=0}^{\mathscr{M}}\alpha_{i,j}\hat{m}_i\hat{m}_j\right| &= \left|\zeta_j^{(1)}\hat{m}_j + \frac{h^{-\nu}}{\Gamma(2-\nu)}\sum_{r=1}^{j-1}(\sigma_r - \sigma_{r+1})\hat{m}_{j-r}\hat{m}_j\right| \\ &\leq \left|\zeta_j^{(1)}\right|\left|\hat{m}_j\right| + \frac{h^{-\nu}}{\Gamma(2-\nu)}\sum_{r=1}^{j-1}(\sigma_r - \sigma_{r+1})\left|\hat{m}_{j-r}\right|\left|\hat{m}_j\right|\end{aligned}$$

Since all terms on L.H.S are positive, we have

$$\frac{h^{-\nu}}{\Gamma(2-\nu)}\left|\hat{m}_j^2\right| \leq \left|\zeta_j^{(1)}\right|\left|\hat{m}_j\right| + \frac{h^{-\nu}}{\Gamma(2-\nu)}\sum_{r=1}^{j-1}(\sigma_r - \sigma_{r+1})\left|\hat{m}_{j-r}\right|\left|\hat{m}_j\right|.$$

Dividing both sides by $\left|\hat{m}_j\right|$, we get

$$\frac{h^{-\nu}}{\Gamma(2-\nu)}\left|\hat{m}_j\right| \leq \left|\zeta_j^{(1)}\right| + \frac{h^{-\nu}}{\Gamma(2-\nu)}\sum_{r=1}^{j-1}(\sigma_r - \sigma_{r+1})\left|\hat{m}_{j-r}\right|.$$

Therefore,

$$L_1 p\mathcal{D}^\nu\left|\hat{m}_j\right| \leq \left|\zeta_j^{(1)}\right|.$$

Since $\sigma_1 = 1$ and $\sigma_l > \sigma_{l+1}$ for all $l \geq 1$, by the mean value theorem [44], we have

$$(1-\nu)l^{-\nu} \leq \sigma_l \leq (1-\nu)(l-1)^{-\nu}, \text{ for } l \geq 2.$$

Using Lemma 4.1, we get

$$\begin{aligned}\left|\hat{m}_j\right| &\leq \max_{1\leq r\leq j}\left\{\frac{h^{-\nu}\Gamma(2-\nu)}{\sigma_r}\left|\zeta_r^{(1)}\right|\right\} \\ &\leq \frac{h^\nu\Gamma(2-\nu)}{(1-\nu)\mathscr{M}^{-\nu}}\max_{1\leq r\leq j}\left\{\left|\zeta_r^{(1)}\right|\right\} \\ &= T^\nu\Gamma(1-\nu)\max_{1\leq r\leq j}\left\{\left|\zeta_r^{(1)}\right|\right\}, \quad j = 1, \cdots, \mathscr{M}.\end{aligned}$$

This implies that

$$\|\hat{E}\|_\infty \leq T^\nu\Gamma(1-\nu)\left\|\zeta^{(1)}\right\|_\infty.$$

□

Theorem 4.2. *Suppose that* $\{\hat{\mathcal{Y}}_j\}_{j=0}^{\mathscr{M}}$ *is numerical solution of (1.1) obtained by using Scheme-I (3.12) and* $\{\mathcal{Y}(t_j)\}_{j=0}^{\mathscr{M}}$ *be the analytical solution, then*

$$\max_{1\leq j\leq\mathscr{M}}\|\mathcal{Y}(t_j) - \hat{\mathcal{Y}}_j\| \leq CT^\nu h^{2-\nu}.$$

Proof. By Lemmas 4.2 and 4.3, we have

$$\begin{aligned}\left|\zeta_j^{(1)}\right| &\le \left|\zeta_j^{(L1)}\right| + \left|\zeta_j^{(P)}\right| \\ &\le C\left(h^{2-\nu} + h^{\mathcal{M}+1}\right).\end{aligned}$$

Now, by Theorem 4.1, we have

$$\begin{aligned}\max_{1\le j\le \mathcal{M}} \|\mathcal{Y}(t_j) - \hat{\mathcal{Y}}_j\| &\le T^{\nu}\Gamma(1-\nu)\max_{1\le j\le \mathcal{M}}\left|\zeta_j^{(1)}\right| \\ &\le T^{\nu}\Gamma(1-\nu)(h^{2-\nu} + h^{\mathcal{M}+1}) \\ &\le CT^{\nu}h^{2-\nu},\end{aligned}$$

which completes the proof. □

4.2 | Stability and convergence analysis for Scheme-II

Let $\tilde{m}_j = |\mathcal{Y}(t_j) - \tilde{\mathcal{Y}}_j|$ for $j = 1, 2, \cdots, \mathcal{M}$, denote the absolute error at t_j. From (3.19) and (3.21), we get the following difference equations:

$$\begin{cases} L1\text{-}2_p\mathcal{D}^{\nu}\tilde{m}_j + \mathcal{A}_j\tilde{m}_j + \lambda\sum_{i=0}^{\mathcal{M}}\alpha_{i,j}\tilde{m}_i = \zeta_j^2, \text{ for } j = 1, \cdots, \mathcal{M}, \\ \tilde{m}_0 = 0. \end{cases} \tag{4.2}$$

Lemma 4.4. ([9]). *For any mesh function $\{\tilde{\mathcal{Y}}_j\}_{j=0}^{\mathcal{M}}$ with $\tilde{\mathcal{Y}}_0 = 0$, we have*

$$|\tilde{\mathcal{Y}}_j| \le \max_{r=1,3,\ldots,j}\left\{\frac{h^{\nu}\Gamma(2-\nu)}{\rho_r}L1\text{-}2_p\mathcal{D}^{\nu}|\tilde{\mathcal{Y}}_r|\right\}, \quad \textit{for } j = 1, \cdots, \mathcal{M}.$$

Lemma 4.5. ([9]). *If $\mathcal{Y}(t) \in C^3[0, T]$ be the analytical solution of (1.1), then the remainder term of L1-2 approximation (3.16) satisfies*

$$|\zeta_j^{(L1\text{-}2)}| \le Ch^{3-\nu}, \quad j = 1, \cdots, \mathcal{M}.$$

Theorem 4.3. *For the difference Equation 4.2, solution satisfies the following inequality:*

$$\|\tilde{E}\|_{\infty} \le T^{\nu}\Gamma(1-\nu)\|\zeta^{(2)}\|_{\infty},$$

where $\tilde{E} = (\tilde{m}_0, \tilde{m}_1, \cdots, \tilde{m}_{\mathcal{M}})'$, and $\zeta^{(1)} = (\zeta_0^{(2)}, \zeta_1^{(2)}, \cdots, \zeta_{\mathcal{M}}^{(2)})'$.

Proof. In problem (4.2), use (3.16) without remainder term and then multiply by $\tilde{m}_j$ both sides, it follows that

$$\begin{aligned}\left|\frac{h^{-\nu}}{\Gamma(2-\nu)}\rho_1\tilde{m}_j^2 + \mathcal{A}_j\tilde{m}_j^2 + \lambda\sum_{i=0}^{\mathcal{M}}\alpha_{i,j}\tilde{m}_i\tilde{m}_j\right| &= \left|\zeta_j^{(2)}\hat{m}_j + \frac{h^{-\nu}}{\Gamma(2-\nu)}\sum_{\substack{r=1\\ r\ne 2}}^{j-1}(\rho_r - \rho_{r+1})\tilde{m}_{j-r}\tilde{m}_j\right| \\ &\le \left|\zeta_j^{(2)}\right|\left|\tilde{m}_j\right| + \frac{h^{-\nu}}{\Gamma(2-\nu)}\sum_{\substack{r=1\\ r\ne 2}}^{j-1}(\rho_r - \rho_{r+1})\left|\tilde{m}_{j-r}\right|\left|\tilde{m}_j\right|.\end{aligned}$$

Since, $\mathcal{A}_j > 0$ and $\lambda\sum_{i=0}^{\mathcal{M}}\alpha_{i,j}\tilde{m}_i\tilde{m}_j > 0$, we have

$$\frac{h^{-\nu}}{\Gamma(2-\nu)}\rho_1|\tilde{m}_j^2| \le \left|\zeta_j^{(2)}\right|\left|\tilde{m}_j\right| + \frac{h^{-\nu}}{\Gamma(2-\nu)}\sum_{\substack{r=1\\ r\ne 2}}^{j-1}(\rho_r - \rho_{r+1})\left|\tilde{m}_{j-r}\right|\left|\tilde{m}_j\right|.$$

Dividing by $|\tilde{m}_j|$ both sides, we get

$$L1\text{-}2_p\mathcal{D}^\nu|\tilde{m}_j| \le |\zeta_j^{(2)}|.$$

Since, $\rho_1 \in (1, \frac{3}{2})$, $\rho_1 > |\rho_2|$, $\rho_1 > \rho_3$, and $\rho_l \ge \rho_{l+1}\ \forall l \ge 3$, by Lemma 4.4, we have

$$\begin{aligned}
|\tilde{m}_j| &\le \max_{r=1,3,\dots,j}\left\{\frac{h^{-\nu}\Gamma(2-\nu)}{\rho_r}\left|\zeta_r^{(2)}\right|\right\} \\
&\le \frac{h^\nu\Gamma(2-\nu)}{(1-\nu)\mathcal{M}^{-\nu}}\max_{r=1,3,\cdots,j}\left\{\left|\zeta_r^{(2)}\right|\right\} \\
&= T^\nu\Gamma(1-\nu)\max_{r=1,3,\cdots,j}\left\{\left|\zeta_r^{(2)}\right|\right\}.
\end{aligned}$$

This proves the theorem. □

Theorem 4.3 shows that the Scheme-II is stable.

Theorem 4.4. *If $\{\mathcal{Y}(t_j)\}_{j=0}^{\mathcal{M}}$ be the analytical solution and $\{\tilde{\mathcal{Y}}_j\}_{j=0}^{\mathcal{M}}$ be the approximate solution of the model (1.1) obtained by using Scheme-II, then*

$$\|\tilde{E}\|_\infty \le CT^\nu h^{3-\nu}.$$

Proof. From Lemmas 4.3 and 4.5, we have the following inequality:

$$|\zeta_j^{(2)}| \le \left|\zeta_j^{(L1\text{-}2)}\right| + \left|\zeta_j^{(P)}\right| \le C(h^{3-\nu} + h^{\mathcal{M}+1}).$$

By Theorem 4.3, we get

$$\begin{aligned}
\max_{1\le j\le\mathcal{M}}\|\mathcal{Y}(t_j) - \tilde{\mathcal{Y}}_j\| &\le T^\nu\Gamma(1-\nu)\|\zeta^{(2)}\|_\infty \\
&\le T^\nu\Gamma(1-\nu)(h^{3-\nu} + h^{\mathcal{M}+1}) \\
&\le CT^\nu h^{3-\nu}.
\end{aligned}$$

□

Remark 4.1. Observe from Lemmas 4.1 and 4.4 that the solution is bounded by its derivatives because the proposed model (1.1) is not time singular problem and has a sufficiently smooth solution, leading to a stable solution.

5 | NUMERICAL EXPERIMENTS

This section describes several numerical experiments conducted to validate the theoretical findings, effectiveness, and accuracy of the proposed methods.

We have solved three test problems involving FOVIDE. The first and the third problems are taken to compare the numerical results obtained by the proposed schemes with the numerical results provided by the existing method [9]. The second problem is taken with a weakly singular kernel. The analytical solution is provided to show the validity of the numerically obtained solution. Different tables and graphs are given, depicting the numerical outcomes of the presented method. The accuracy of the proposed approach is found for different cases by using pointwise absolute errors $\mathcal{E}_{\mathcal{M}}(i)$, L_2-errors, and maximum errors $\Xi_{\mathcal{M}}$ defined by

$$\begin{cases}
\mathcal{E}_{\mathcal{M}}(i) = |\mathcal{Y}(t_i) - \mathcal{Y}_{\mathcal{M}}(t_i)|, \quad i = 0, \cdots, \mathcal{M}, \\
L_2 - error = \sqrt{\sum_{i=0}^{\mathcal{M}} h(\mathcal{E}_{\mathcal{M}}(i))^2}, \\
\Xi_{\mathcal{M}} = \max_{0\le i\le\mathcal{M}}\mathcal{E}_{\mathcal{M}}(i).
\end{cases} \tag{5.1}$$

Here, $\mathcal{Y}(t)$ is the exact solution and $\mathcal{Y}_{\mathcal{M}}(t)$ denotes the numerical solution obtained using numerical method. Formula used to calculate the corresponding order of convergence is defined by

$$\mathscr{C}_{\mathcal{M}} = \log_2\left(\frac{\Xi_{\mathcal{M}}}{\Xi_{2\mathcal{M}}}\right). \tag{5.2}$$

TABLE 1 Comparison of $\Xi_{\mathcal{M}}$ and $\mathscr{C}_{\mathcal{M}}$ by using Scheme-II and Scheme-I with different values of ν and $\mathcal{M}$ for Example 5.1.

		Scheme-I		Scheme-II	
ν	$\mathcal{M}$	$\Xi_{\mathcal{M}}$	$\mathscr{C}_{\mathcal{M}}$	$\Xi_{\mathcal{M}}$	$\mathscr{C}_{\mathcal{M}}$
0.2	32	2.1551e−04	-	7.2370e−06	-
	64	6.6112e−05	1.7048	1.1162e−06	2.6968
	128	2.0040e−05	1.7220	1.6952e−07	2.7191
	256	6.0187e−06	1.7354	2.7397e−08	2.6294
	512	1.7944e−06	1.7460	3.7998e−09	2.8500
0.4	32	1.1000e−03	-	3.3804e−05	-
	64	3.6845e−04	1.5780	5.7805e−06	2.5479
	128	1.2453e−04	1.5650	9.7779e−07	2.5636
	256	4.1819e−05	1.5743	1.6419e−07	2.5742
	512	1.3979e−05	1.5809	2.7437e−08	2.5812
0.6	32	4.2000e−03	-	1.3268e−04	-
	64	1.6000e−03	1.3923	2.5627e−05	2.3227
	128	6.1939e−04	1.3692	4.9113e−06	2.3835
	256	2.3668e−04	1.3879	9.3704e−07	2.3899
	512	9.0159e−05	1.3924	1.7830e−07	2.3938
0.8	32	1.3500e−02	-	5.0523e−04	-
	64	6.0000e−03	1.1699	1.1127e−04	2.1829
	128	2.6000e−03	1.2065	2.4370e−05	2.1909
	256	1.1000e−03	1.2410	5.3212e−06	2.1953
	512	5.0146e−04	1.1333	1.1601e−06	2.1975

TABLE 2 Comparison of $\Xi_{\mathcal{M}}$ and $\mathscr{C}_{\mathcal{M}}$ obtained by Scheme-I and by existing L1 method [9] for Example 5.1 with different values of ν and $\mathcal{M}$.

		Scheme-I		Existing L1 scheme	
ν	$\mathcal{M}$	$\Xi_{\mathcal{M}}$	$\mathscr{C}_{\mathcal{M}}$	$\Xi_{\mathcal{M}}$	$\mathscr{C}_{\mathcal{M}}$
0.2	32	2.1551e−04	-	3.3773e−04	-
	64	5.6112e−05	1.7048	7.3160e−05	2.2067
	128	2.0040e−05	1.7220	1.5050e−05	2.2820
	256	6.0187e−06	1.7354	3.3970e−06	2.1470
	512	1.7944e−06	1.7460	1.0940e−06	1.6350
0.4	32	1.1000e−03	-	7.1461e−04	-
	64	3.6845e−04	1.5780	2.7080e−04	1.3999
	128	1.2453e−04	1.5650	9.8730e−05	1.4550
	256	4.1819e−05	1.5743	3.5080e−05	1.4930
	512	1.3979e−05	1.5809	1.2230e−05	1.5200
0.6	32	4.2000e−03	-	3.6000e−03	-
	64	1.6000e−03	1.3923	1.4820e−03	1.2805
	128	6.1939e−04	1.3692	5.8660e−04	1.3370
	256	2.3668e−04	1.3879	2.2850e−04	1.3600
	512	9.0159e−05	1.3924	8.8110e−05	1.3750
0.8	32	1.3500e−02	-	1.3000e−02	-
	64	6.0000e−03	1.1699	5.8640e−03	1.1486
	128	2.6000e−03	1.2065	2.5980e−03	1.1750
	256	1.1000e−03	1.2410	1.1420e−03	1.1860
	512	5.0146e−04	1.1333	4.9960e−04	1.1920

TABLE 3 Comparison of $\Xi_{\mathscr{M}}$ and $\mathscr{C}_{\mathscr{M}}$ obtained by Scheme-II and by existing L1-2 method [9] for Example 5.1 with different values of ν and $\mathscr{M}$.

		Scheme-II		Existing L1-2 scheme	
ν	$\mathscr{M}$	$\Xi_{\mathscr{M}}$	$\mathscr{C}_{\mathscr{M}}$	$\Xi_{\mathscr{M}}$	$\mathscr{C}_{\mathscr{M}}$
0.1	32	2.4886e−06	-	5.3560e−04	-
	64	3.6843e−07	2.7559	1.3400e−04	1.9999
	128	5.3590e−08	2.7814	3.3500e−05	2.0000
	256	7.7102e−09	2.7971	8.3760e−06	2.0000
	512	1.0960e−09	2.8145	2.0940e−06	2.0000
0.3	32	1.6320e−05	-	5.4380e−04	-
	64	2.6443e−06	2.6257	1.3660e−04	1.9930
	128	4.2253e−07	2.6458	3.4230e−05	1.9960
	256	6.6930e−08	2.6583	8.5710e−06	1.9980
	512	1.0535e−08	2.6670	2.1450e−06	1.9990
0.5	32	6.7505e−05	-	4.9600e−04	-
	64	1.2248e−05	2.4634	1.2730e−04	1.9630
	128	2.2017e−06	2.4759	3.2380e−05	1.9750
	256	3.9356e−07	2.4840	8.1950e−06	1.9820
	512	7.0092e−08	2.4893	2.0660e−06	1.9880
0.7	32	2.5915e−04	-	2.669e−04	-
	64	5.3407e−05	2.2787	7.7520e−05	1.7840
	128	1.0934e−05	2.2882	2.1590e−05	1.8440
	256	2.2305e−06	2.2934	5.8500e−06	1.8840
	512	4.5414e−07	2.2962	1.5550e−06	1.9120
0.9	32	9.8516e−04	-	7.1760e−04	-
	64	2.3219e−04	2.0851	1.6900e−04	2.0860
	128	5.4441e−05	2.0926	3.9280e−05	2.1050
	256	1.2731e−05	2.0963	9.0690e−06	2.1150
	512	2.9736e−06	2.0981	2.0870e−06	2.1200

Remark 5.1. For the sake of convenience, $\tilde{\mathcal{Y}}^i_{\mathscr{M}}$ and $\hat{\mathcal{Y}}^i_{\mathscr{M}}$ given below in different graphical representation denotes the numerical solution obtained for different values of $\mathscr{M}$ by Scheme-II and Scheme-I, respectively, when the value of ν is chosen as $\nu = 0.i$, $i = 1, \cdots, 9$.

Remark 5.2. We used (a) an 11th Gen Intel(R) Core(TM) i5-11320H @ 3.20GHz 2.50 GHz, (b) 8.00 GB of RAM to conduct our numerical tests (7.74 GB usable), and (c) system specifications include a 64-bit operating system, an x64-based CPU, and MATLAB R2023b (The MathWorks, Inc., Natick, Massachusetts) programming environment.

Example 5.1. In the model problem (1.1), let $\mathcal{K}(t,s) = 3t + 4s$, $\lambda = 1$, $\mathcal{A}(t) = 1$ under the initial condition $\mathcal{Y}(0) = 0$. We choose

$$\mathcal{G}(t) = \pi\nu \frac{(1+\nu)(2+\nu)(3+\nu)t^3 \csc(\pi\nu)}{6\Gamma(1-\nu)} + t^{3+\nu} + \frac{(7\nu+31)t^{5+\nu}}{(4+\nu)(5+\nu)},$$

so that analytical solution is $\mathcal{Y}(t) = t^{3+\nu}$.

Following Algorithms 1 and 2 for Example 5.1, the numerical outcomes of different experiments are illustrated below:

- In Table 1, efficiency of the Scheme-I and Scheme-II is demonstrated by comparing maximum error and order of convergence of both the two schemes. It can be seen for the table that the order of convergence of Scheme-I and Scheme-II is near to $(2-\nu)$ and $(3-\nu)$, respectively.
- Table 2 shows the comparison of $\Xi_{\mathscr{M}}$ and $\mathscr{C}_{\mathscr{M}}$ by using the presented Scheme-I and existing L1 method. Observe that the order of convergence of the presented Scheme-I is better than the existing L1 method.
- In Table 3, comparison of $\Xi_{\mathscr{M}}$ and $\mathscr{C}_{\mathscr{M}}$ by using the presented Scheme-II and the existing L1-2 method is shown. It can be seen that $\Xi_{\mathscr{M}}$, and $\mathscr{C}_{\mathscr{M}}$ of the present Scheme-II is better then the existing L1-2 method.
- In Figure 1, comparison of $\mathcal{Y}$, $\hat{\mathcal{Y}}^1_{\mathscr{M}}$ and $\tilde{\mathcal{Y}}^1_{\mathscr{M}}$ is shown in case of Example 5.1 for $\mathscr{M} = 128$. To accurately illustrate the characteristics of the solution graph, we multiply $\hat{\mathcal{Y}}^1_{\mathscr{M}}$ and $\tilde{\mathcal{Y}}^1_{\mathscr{M}}$ by the quantity 1.1 and 1.3, respectively.
- Figure 2 shows the variation of numerical solutions $\hat{\mathcal{Y}}^1_{\mathscr{M}}$, $\hat{\mathcal{Y}}^3_{\mathscr{M}}$, $\hat{\mathcal{Y}}^5_{\mathscr{M}}$, $\hat{\mathcal{Y}}^7_{\mathscr{M}}$, and $\hat{\mathcal{Y}}^9_{\mathscr{M}}$ with $\mathscr{M} = 128$.

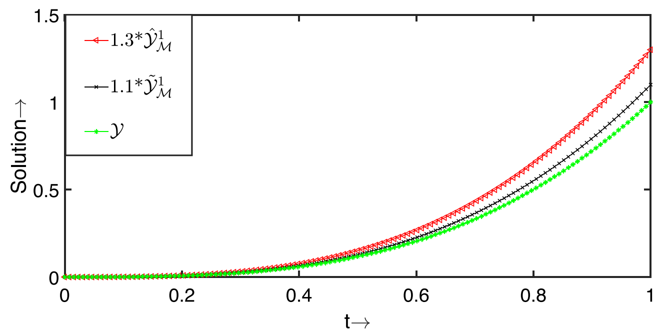

FIGURE 1 Comparison between the approximate and exact solutions for Example 5.1 with $\mathcal{M} = 128$. [Colour figure can be viewed at wileyonlinelibrary.com]

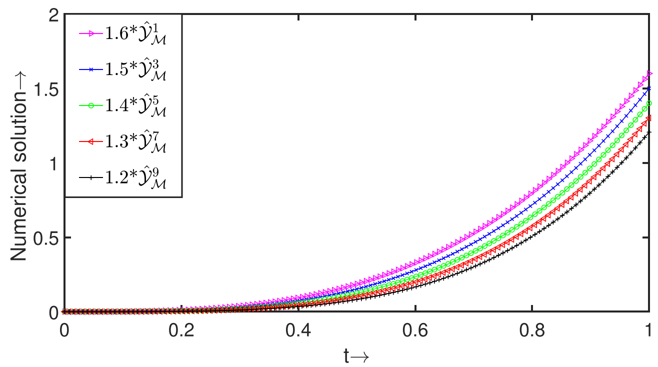

FIGURE 2 Graph for numerical solution of Scheme-I with $\mathcal{M} = 128$ for Example 5.1. [Colour figure can be viewed at wileyonlinelibrary.com]

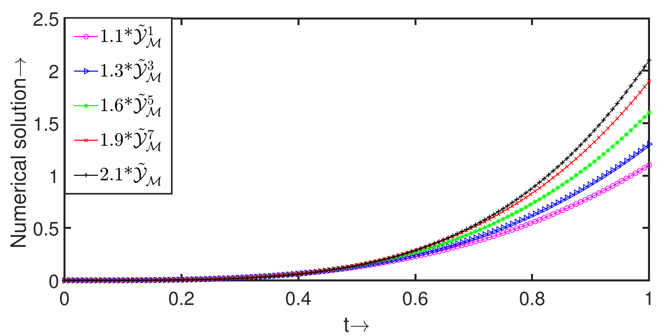

FIGURE 3 Graph for numerical solution of Scheme-II with $\mathcal{M} = 128$ for Example 5.1. [Colour figure can be viewed at wileyonlinelibrary.com]

- Figure 3 shows the graphical representation of behavior of the solution $\tilde{\mathcal{Y}}^1_{\mathcal{M}}$, $\tilde{\mathcal{Y}}^3_{\mathcal{M}}$, $\tilde{\mathcal{Y}}^5_{\mathcal{M}}$, $\tilde{\mathcal{Y}}^7_{\mathcal{M}}$, and $\tilde{\mathcal{Y}}^9_{\mathcal{M}}$ with $\mathcal{M} = 128$.
- To show the variation of numerical solution precisely, we labeled the graphs in Figures 2 and 3. In Figure 2, we multiply $\hat{\mathcal{Y}}^1_{\mathcal{M}}$, $\hat{\mathcal{Y}}^3_{\mathcal{M}}$, $\hat{\mathcal{Y}}^5_{\mathcal{M}}$, $\hat{\mathcal{Y}}^7_{\mathcal{M}}$, and $\hat{\mathcal{Y}}^9_{\mathcal{M}}$ with 1.6, 1.5, 1.9, 1.3 and 1.2, respectively. Similarly, in Figure 3, we multiply $\tilde{\mathcal{Y}}^3_{\mathcal{M}}$, $\tilde{\mathcal{Y}}^5_{\mathcal{M}}$, $\tilde{\mathcal{Y}}^7_{\mathcal{M}}$, and $\tilde{\mathcal{Y}}^9_{\mathcal{M}}$ by 1.1, 1.3, 1.9, and 2.1, respectively.

Example 5.2. The second test problem is considered as the following model

$$\begin{cases} \mathcal{D}^{\nu}_t \mathcal{Y}(t) + \mathcal{Y}(t) + \int_0^t \mathcal{K}(t,s)\mathcal{Y}(s)ds = \mathcal{G}(t), \;\; t \in (0,1], \\ \mathcal{Y}(0) = 0, \end{cases} \tag{5.3}$$

with weakly singular kernel

$$\mathcal{K}(t,s) = \frac{1}{(t-s)^{\beta}}, \;\; \beta \in (0,1),$$

and

$$\mathcal{G}(t) = 5040\frac{t^{7-\nu}}{\Gamma(8-\nu)} + t^7 + 5040\Gamma(1-\beta)\frac{t^{8-\beta}}{\Gamma(9-\beta)},$$

the analytical solution of this test problem is given by $\mathcal{Y}(t) = t^7$.

After following Algorithms 1 and 2 for the above test problem, the numerical outcomes obtained for different values of ν and $\beta = 0.95$, are illustrated below:

TABLE 4 Results of absolute error of Example 5.2 for $\mathcal{M} = 50$ and $\nu = 0.1$.

	Scheme-I		Scheme-II	
t	$\hat{\mathcal{y}}^1_{\mathcal{M}}$	$\mathcal{E}_{\mathcal{M}}$	$\tilde{\mathcal{y}}^1_{\mathcal{M}}$	$\mathcal{E}_{\mathcal{M}}$
0.1	0.00000010..	2.6394e−12	0.00000010..	8.4997e−13
0.2	0.00001280..	1.0000e−08	0.00001280..	8.0000e−10
0.3	0.00021874..	4.0000e−08	0.00021870..	4.7000e−09
0.4	0.00163858..	1.9000e−07	0.00163841..	1.5800e−08
0.5	0.00781309..	5.9000e−07	0.00781254..	4.0300e−08
0.6	0.02799512..	1.5200e−06	0.02799368..	8.6100e−08
0.7	0.08235766..	3.3600e−06	0.08235446..	1.6330e−07
0.8	0.20972187..	6.6800e−06	0.20971548..	2.8390e−07
0.9	0.47830911..	1.2200e−05	0.47829736..	4.6180e−07
1.0	1.00002095..	2.0960e−05	1.00000071..	7.1320e−07

TABLE 5 Comparison of $\Xi_{\mathcal{M}}$ and $\mathcal{C}_{\mathcal{M}}$ by using Scheme-I and Scheme-II for Example 5.2.

		Scheme-I		Scheme-II	
ν	$\mathcal{M}$	$\Xi_{\mathcal{M}}$	$\mathcal{C}_{\mathcal{M}}$	$\Xi_{\mathcal{M}}$	$\mathcal{C}_{\mathcal{M}}$
0.2	10	1.8000e−03	-	4.5107e−04	-
	20	6.1374e−04	1.5523	8.2338e−05	2.4537
	40	2.0099e−04	1.6105	1.3774e−05	2.5796
	80	6.3688e−05	1.6580	2.1955e−06	2.6493
0.4	10	6.2000e−3	-	1.6000e−03	-
	20	2.4000e−03	1.3692	3.2774e−04	2.2874
	40	8.5943e−04	1.4816	6.0853e−05	2.4292
	80	3.0195e−04	1.5091	1.0784e−05	2.4964
0.6	10	1.6100e−02	-	4.3000e−03	-
	20	6.9000e−03	1.2224	9.8409e−04	2.1275
	40	2.8000e−03	1.3012	2.0545e−04	2.2600
	80	1.1000e−03	1.3479	4.1057e−05	2.3231
0.8	10	3.6700e−02	-	1.0200e−02	-
	20	1.7500e−02	1.0684	2.6000e−03	1.9720
	40	8.0000e−03	1.1293	6.2048e−04	2.0671
	80	3.6000e−03	1.1520	1.4105e−04	2.1372

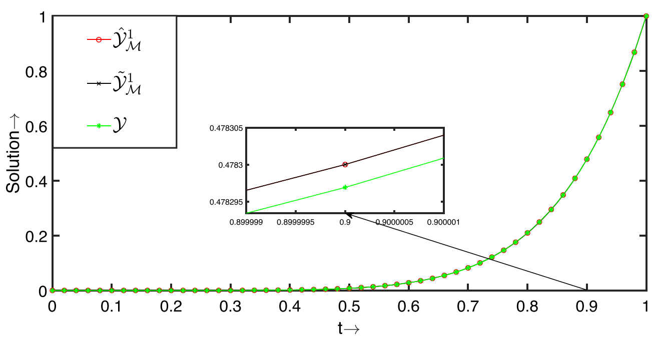

FIGURE 4 Comparison between the exact and the approximate solution with $\mathcal{M} = 50$ and $\nu = 0.1$ for Example 5.2. [Colour figure can be viewed at wileyonlinelibrary.com]

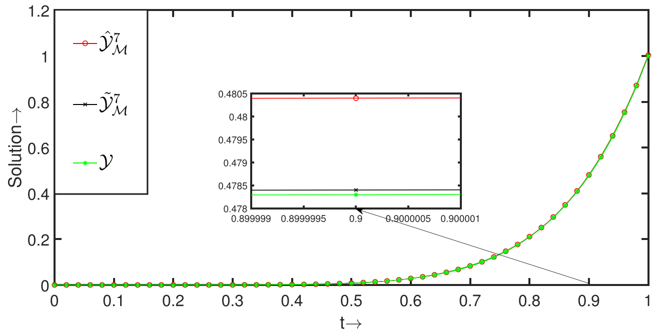

FIGURE 5 Comparison between the exact and the approximate solution with $\mathscr{M} = 50$ and $\nu = 0.7$ for Example 5.2. [Colour figure can be viewed at wileyonlinelibrary.com]

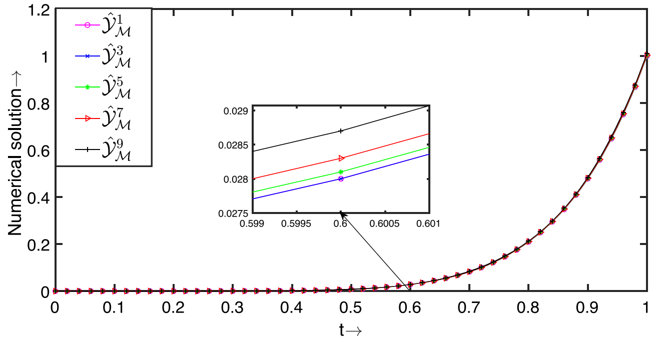

FIGURE 6 Approximate solution with $\mathscr{M} = 50$ obtained via Scheme-I for Example 5.2. [Colour figure can be viewed at wileyonlinelibrary.com]

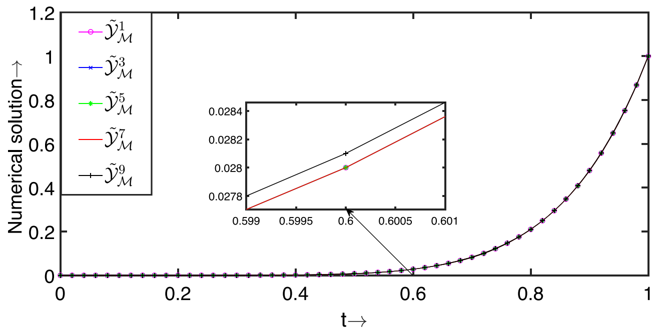

FIGURE 7 Approximate solution with $\mathscr{M} = 50$ obtained via Scheme-II for Example 5.2. [Colour figure can be viewed at wileyonlinelibrary.com]

- Variation of pointwise error $\mathcal{E}_{\mathscr{M}}$ of numerical solutions $\tilde{\mathcal{Y}}^1_{\mathscr{M}}$, and $\hat{\mathcal{Y}}^1_{\mathscr{M}}$, obtained by Scheme-II and Scheme-I respectively, with $\nu_1 = 0.1$ and $\mathscr{M} = 80$ is provided in Table 4. Observe that for the point close to 0, absolute error is very small and increases for the points close to 1. Also, the absolute error for the Scheme-II is small as compared to the Scheme-I.
- In Table 5, efficiency of the Scheme-I and Scheme-II is demonstrated by comparing maximum error $\Xi_{\mathscr{M}}$ and order of convergence $\mathscr{C}_{\mathscr{M}}$ of both schemes. Observe that the order of convergence for Scheme-I and Scheme-II is near to $(2-\nu)$ and $(3-\nu)$, respectively.
- Figure 4 depicts the comparison of exact analytical solution $\mathcal{Y}$ and numerical solutions ($\tilde{\mathcal{Y}}^1_{\mathscr{M}}$ and $\hat{\mathcal{Y}}^1_{\mathscr{M}}$), obtained via Scheme-II and Scheme-I for $\nu = 0.1$ with $\mathscr{M} = 50$.
- Variation of analytical solution $\mathcal{Y}$ and numerical solutions ($\tilde{\mathcal{Y}}^7_{\mathscr{M}}$ and $\hat{\mathcal{Y}}^7_{\mathscr{M}}$) obtained by using Scheme-II and Scheme-I for $\nu = 0.7$ with $\mathscr{M} = 50$. is shown in Figure 5.
- From Figures 4 and 5, it is observed that accuracy of the numerical solution for both Scheme-II and Scheme-I varies with ν.

TABLE 6 Comparison of $\Xi_{\mathscr{M}}$ and $\mathscr{C}_{\mathscr{M}}$ by using Scheme-II and Scheme-I with different values of ν and $\mathscr{M}$ for Example 5.3.

		Scheme-I		Scheme-II	
ν	$\mathscr{M}$	$\Xi_{\mathscr{M}}$	$\mathscr{C}_{\mathscr{M}}$	$\Xi_{\mathscr{M}}$	$\mathscr{C}_{\mathscr{M}}$
0.2	16	5.9520e−04	-	2.3462e−04	-
	32	1.8739e−04	1.6673	4.2821e−05	2.4539
	64	5.7801e−05	1.6969	7.1146e−06	2.5895
	128	1.7584e−05	1.7168	1.1279e−06	2.6571
0.4	16	1.8000e−03	-	2.6996e−04	-
	32	6.1673e−04	1.5453	6.1867e−05	2.1255
	64	2.1165e−04	1.5430	1.2136e−05	2.3499
	128	7.1793e−05	1.5598	2.2113e−06	2.4563
0.6	16	4.0000e−03	-	3.7348e−04	-
	32	1.6000e−03	1.3219	7.2729e−05	2.3604
	64	6.1278e−04	1.3846	1.3929e−05	2.3844
	128	2.3544e−04	1.3800	2.6565e−06	2.3905
0.8	16	7.8000e−03	-	8.3477e−04	-
	32	3.5000e−03	1.1561	1.8547e−04	2.1702
	64	1.5000e−03	1.2224	4.0626e−05	2.1907
	128	6.7938e−04	1.1427	8.8632e−06	2.1965

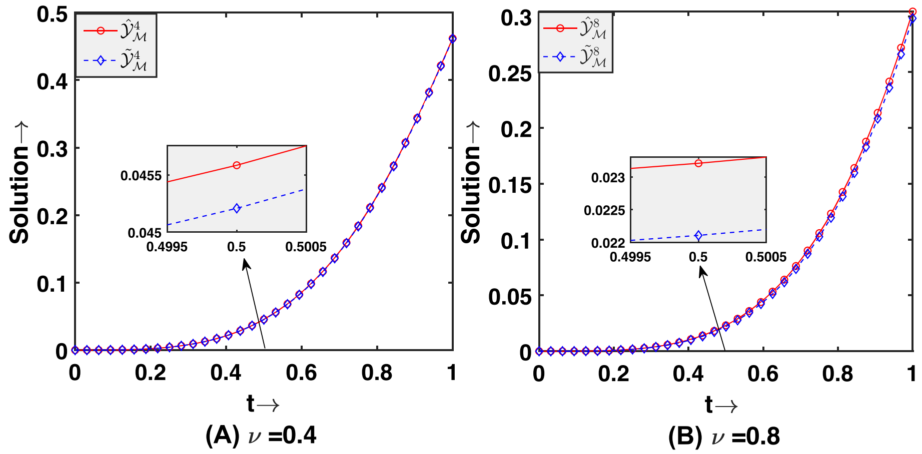

FIGURE 8 Comparison between the Scheme-I and Scheme-II solutions for Example 5.3 with $\mathscr{M}$ = 32. [Colour figure can be viewed at wileyonlinelibrary.com]

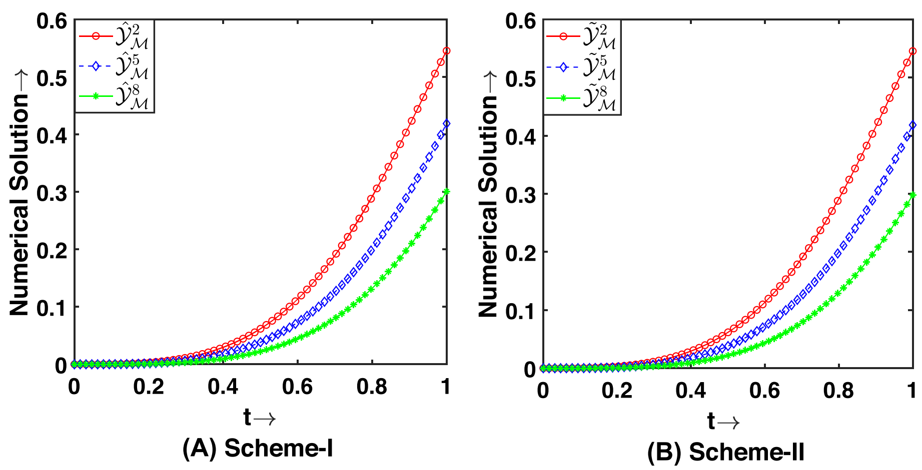

FIGURE 9 Numerical solution obtained via Scheme-I and Scheme-II for Example 5.3 with $\mathscr{M}$ = 64 and different values of ν. [Colour figure can be viewed at wileyonlinelibrary.com]

- Variation in solution graph $\hat{\mathcal{Y}}^1_{\mathscr{M}}$, $\hat{\mathcal{Y}}^3_{\mathscr{M}}$, $\hat{\mathcal{Y}}^5_{\mathscr{M}}$, $\hat{\mathcal{Y}}^7_{\mathscr{M}}$, and $\hat{\mathcal{Y}}^9_{\mathscr{M}}$ obtained via Scheme-I with $\mathscr{M} = 50$ is shown in Figure 6.
- Figure 7 shows the graphical representation of behavior of the solution $\tilde{\mathcal{Y}}^1_{\mathscr{M}}$, $\tilde{\mathcal{Y}}^3_{\mathscr{M}}$, $\tilde{\mathcal{Y}}^5_{\mathscr{M}}$, $\tilde{\mathcal{Y}}^7_{\mathscr{M}}$, and $\tilde{\mathcal{Y}}^9_{\mathscr{M}}$ obtained by using Scheme-II with $\mathscr{M} = 50$.

Example 5.3. Consider the FOVIDE

$$\begin{cases} \mathcal{D}_t^{\nu}\mathcal{Y}(t) + (1-t)\mathcal{Y}(t) + \int_0^t [s^3 e^t + t\sin^2(t)]\mathcal{Y}(s)ds = t^3, \ t \in (0,1], \\ \mathcal{Y}(0) = 0. \end{cases} \tag{5.4}$$

The exact solution is unknown.

We use the double mesh principle to calculate the maximum error as

$$\Xi_{\mathscr{M}} = \max_{0 \le j \le \mathscr{M}} |\mathcal{Y}_j - \mathcal{Y}_{2j}|,$$

where $\mathcal{Y}_j$ is approximate solution.

Now, following Algorithms 1 and 2 for Example 5.3, the numerical results obtained for different experiments are illustrated below:

- In Table 6, the efficiency of Scheme-I and Scheme-II is demonstrated by comparing the maximum error $\Xi_{\mathscr{M}}$ and the order of convergence $\mathscr{C}_{\mathscr{M}}$ of both schemes. The table shows that the order of convergence for Scheme-I and Scheme-II is approximately $(2-\nu)$ and $(3-\nu)$, respectively. When these results are compared with the existing method [9] for this problem, it is evident that the proposed schemes perform better.
- Figure 8 provides a comparison of the performance of Scheme-I and Scheme-II. Figure 8A shows the comparison of solutions obtained by Scheme-I and Scheme-II for $\nu = 0.4$, while Figure 8B presents the comparison of solutions obtained by Scheme-I and Scheme-II for $\nu = 0.8$.
- Figure 9 illustrates the variation in numerical solutions obtained by Scheme-I and Scheme-II for different values of ν. Figure 9A shows the variation in solutions obtained by Scheme-I for $\nu = 0.2, 0.5$, and 0.8, while Figure 9B presents the variation in solutions obtained by Scheme-II for $\nu = 0.2, 0.5$, and 0.8.

6 | NUMERICAL STABILITY

In this part, the numerical stability of the proposed schemes is examined. Schemes are implemented on the two test problems with perturbed initial conditions. Perturbation is done by adding the small noise 10 % and 20 % of L_2-error. The numerical results obtained are given in Tables 7–12. Figures 10–13 are also given to show graphically the behavior of the absolute error for different cases.

Remark 6.1. Here, for Scheme-I, $\mathcal{E}^{0\%}$, $\mathcal{E}^{10\%}$, and $\mathcal{E}^{20\%}$ denote the absolute error with 0%, 10%, and 20% noisy data, respectively. Similarly, for Scheme-II, $\tilde{\mathcal{E}}^{0\%}$, $\tilde{\mathcal{E}}^{10\%}$, and $\tilde{\mathcal{E}}^{20\%}$ denote the absolute error with 0%, 10%, and 20% noisy data, respectively.

TABLE 7 Table for pointwise error, L_2- error, and $\Xi_{\mathscr{M}}$ for $\nu = 0.5$ of Example 5.1 with 0% noisy data.

	Scheme-I $\mathcal{E}^{0\%}$			Scheme-II $\tilde{\mathcal{E}}^{0\%}$		
t	$\mathscr{M} = 60$	$\mathscr{M} = 120$	$\mathscr{M} = 240$	$\mathscr{M} = 60$	$\mathscr{M} = 120$	$\mathscr{M} = 240$
0.00	0	0	0	0	0	0
0.20	7.6106e−05	2.8485e−05	1.0460e−05	7.1577e−06	1.3343e−06	2.4341e−07
0.40	2.7824e−04	1.0214e−04	3.7028e−05	1.2380e−05	2.2518e−06	4.0524e−07
0.60	5.3298e−04	1.9394e−04	6.9903e−05	1.4358e−05	2.5838e−06	4.6207e−07
0.80	7.5252e−04	2.7224e−04	9.7749e−05	1.2936e−05	2.3085e−06	4.1074e−07
1.00	8.6770e−04	3.1242e−04	1.1183e−04	9.0348e−06	1.5959e−06	2.8217e−07
L_2-error	5.1653e−04	1.8597e−04	6.6629e−05	1.1212e−05	2.0199e−06	3.6151e−07
$\Xi_{\mathscr{M}}$	8.6770e−04	3.1242e−04	1.1183e−04	1.4363e−05	2.5839e−06	4.6207e−07

TABLE 8 Table for pointwise error, L_2- error, and $\Xi_{\mathcal{M}}$ for $\nu = 0.5$ of Example 5.1 with 10% noisy data.

	Scheme-I $\mathcal{E}^{10\%}$			**Scheme-II** $\tilde{\mathcal{E}}^{10\%}$		
t	$\mathcal{M} = 60$	$\mathcal{M} = 120$	$\mathcal{M} = 240$	$\mathcal{M} = 60$	$\mathcal{M} = 120$	$\mathcal{M} = 240$
0.00	5.1653e−04	1.8597e−05	6.6629e−06	1.1212e−06	2.0199e−07	3.6151e−07
0.20	1.0798e−04	3.9917e−05	1.4548e−05	7.8502e−06	1.4585e−06	2.6560e−07
0.40	2.9970e−04	1.0985e−04	3.9791e−05	1.2846e−05	2.3356e−06	4.2023e−07
0.60	5.4319e−04	1.9762e−04	7.1224e−05	1.4579e−05	2.6238e−06	4.6924e−07
0.80	7.5223e−04	2.7215e−04	9.7720e−05	1.2930e−05	2.3075e−06	4.1058e−07
1.00	8.5993e−04	3.0964e−04	1.1083e−04	8.8655e−06	1.5656e−06	2.7679e−07
L_2-error	5.2105e−04	1.8765e−04	6.7245e−05	1.1461e−05	2.0659e−06	3.6986e−07
$\Xi_{\mathcal{M}}$	8.5993e−04	3.0964e−04	1.1083e−04	1.4579e−05	2.6244e−06	4.6948e−07

TABLE 9 Table for pointwise error, L_2- error, and $\Xi_{\mathcal{M}}$ for $\nu = 0.5$ of Example 5.1 with 20% noisy data.

	Scheme-I $\mathcal{E}^{20\%}$			**Scheme-II** $\tilde{\mathcal{E}}^{20\%}$		
t	$\mathcal{M} = 60$	$\mathcal{M} = 120$	$\mathcal{M} = 240$	$\mathcal{M} = 60$	$\mathcal{M} = 120$	$\mathcal{M} = 240$
0.00	1.0331e−04	3.7194e−05	1.3326e−05	2.2424e−06	4.0398e−07	7.2302e−08
0.20	1.3986e−04	5.1349e−05	1.8636e−05	8.5426e−06	1.5827e−06	2.8778e−07
0.40	3.2116e−04	1.1757e−04	4.2554e−05	1.3312e−05	2.4195e−06	4.3522e−07
0.60	5.5341e−04	2.0131e−04	7.2545e−05	1.4801e−05	2.6638e−06	4.7640e−07
0.80	7.5194e−04	2.7206e−04	9.7691e−04	1.2923e−05	2.3065e−06	4.1042e−07
1.00	8.5215e−04	3.0686e−04	1.0984e−04	8.6963e−06	1.5354e−06	2.7139e−07
L_2-error	5.2655e−04	1.8968e−04	6.7979e−05	1.7220e−05	2.1146e−06	3.7868e−07
$\Xi_{\mathcal{M}}$	8.5215e−04	3.0686e−04	1.0984e−04	1.4812e−05	2.6679e−06	4.7744e−07

TABLE 10 Table for pointwise error, L_2- error, and $\Xi_{\mathcal{M}}$ for $\nu = 0.2$ of Example 5.2 with 0% noisy data.

	Scheme-I $\mathcal{E}^{0\%}$			**Scheme-II** $\tilde{\mathcal{E}}^{0\%}$		
t	$\mathcal{M} = 20$	$\mathcal{M} = 40$	$\mathcal{M} = 80$	$\mathcal{M} = 20$	$\mathcal{M} = 40$	$\mathcal{M} = 80$
0.00	0	0	0	0	0	0
0.20	1.1512e−07	4.5366e−08	1.6044e−08	5.9908e−08	1.3967e−08	2.6594e−09
0.40	4.9699e−06	1.7578e−06	5.8390e−06	1.5296e−06	2.9121e−07	4.9829e−08
0.60	4.2573e−05	1.4459e−05	4.6872e−06	9.1860e−06	1.6299e−06	2.6849e−07
0.80	1.9215e−04	6.3829e−05	2.0410e−05	3.1817e−05	5.4438e−06	8.7883e−07
1.00	6.1374e−04	2.0099e−04	6.3688e−05	8.2338e−05	1.3774e−05	2.1955e−06
L_2-error	2.0799e−04	6.4098e−05	1.0456e−04	2.9892e−05	4.7760e−06	7.4446e−07
$\Xi_{\mathcal{M}}$	6.1374e−04	2.0099e−04	6.3688e−05	8.2338e−05	1.3774e−05	2.1955e−06

TABLE 11 Table for pointwise error, L_2- error, and $\Xi_{\mathcal{M}}$ for $\nu = 0.2$ of Example 5.2 with 10% noisy data.

	Scheme-I $\mathcal{E}^{10\%}$			**Scheme-II** $\tilde{\mathcal{E}}^{10\%}$		
t	$\mathcal{M} = 20$	$\mathcal{M} = 40$	$\mathcal{M} = 80$	$\mathcal{M} = 20$	$\mathcal{M} = 40$	$\mathcal{M} = 80$
0.00	2.0799e−05	6.4098e−06	1.9702e−06	2.9892e−06	4.7760e−07	7446e−08
0.20	1.2706e−06	4.0460e−07	1.2713e−07	2.2674e−07	4.0819e−08	6.8585e−09
0.40	2.9564e−06	2.0639e−06	6.7833e−07	1.6717e−06	3.1405e−07	5.3399e−08
0.60	4.3471e−05	1.4737e−05	4.7730e−06	9.3153e−06	1.6507e−06	2.7174e−07
0.80	1.9299e−04	6.4089e−05	20490e−05	3.1937e−05	5.4632e−06	8.8186e−07
1.00	6.1455e−04	2.0124e−04	6.3764e−05	8.2455e−05	1.3792e−05	2.1984e−06
L_2-error	2.0850e−04	6.4248e−05	1.9746e−05	2.9971e−05	4.7881e−06	7.4631e−07
$\Xi_{\mathcal{M}}$	6.1455e−04	2.0124e−04	6.3764e−05	8.2455e−05	1.3792e−05	2.1984e−06

The numerical results obtained for the first test problem are discussed below:

- Table 7 gives the pointwise error ($\mathcal{E}^{0\%}$ and $\tilde{\mathcal{E}}^{0\%}$), L_2-error, and maximum error $\Xi_{\mathcal{M}}$ for various values of $\mathcal{M}$ and $\nu = 0.5$ with 0% noisy data.

TABLE 12 Table for pointwise error, L_2- error, and $\Xi_{\mathscr{M}}$ for $\nu = 0.2$ of Example 5.2 with 20% noisy data.

	Scheme-I $\mathcal{E}^{20\%}$			**Scheme-II** $\tilde{\mathcal{E}}^{20\%}$		
t	$\mathscr{M} = 20$	$\mathscr{M} = 40$	$\mathscr{M} = 80$	$\mathscr{M} = 20$	$\mathscr{M} = 40$	$\mathscr{M} = 80$
0.00	4.1598e−05	1.2820e−05	3.9402e−06	5.9784e−06	9.5520e−07	1.4889e−07
0.20	2.4260e−06	7.6386e−07	2.3822e−07	3.9358e−07	6.7671e−08	1.1057e−08
0.40	6.9430e−06	2.3700e−06	7.7273e−07	1.8138e−06	3.3689e−07	5.6968e−08
0.60	4.4370e−05	1.5015e−05	4.8588e−06	9.4446e−06	1.6714e−06	2.7498e−07
0.80	1.9383e−04	6.4350e−05	2.0570e−05	3.2058e−05	5.4826e−06	8.8489e−07
1.00	6.1536e−04	1.2820e−05	6.3840e−05	8.2572e−05	1.3811e−05	2.2012e−06
L_2-error	2.0912e−04	6.4415e−05	1.9794e−05	3.0065e−05	4.8014e−06	7.4827e−07
$\Xi_{\mathscr{M}}$	6.1536e−04	2.0148e−04	6.3840e−05	8.2572e−05	1.3811e−05	2.2012e−06

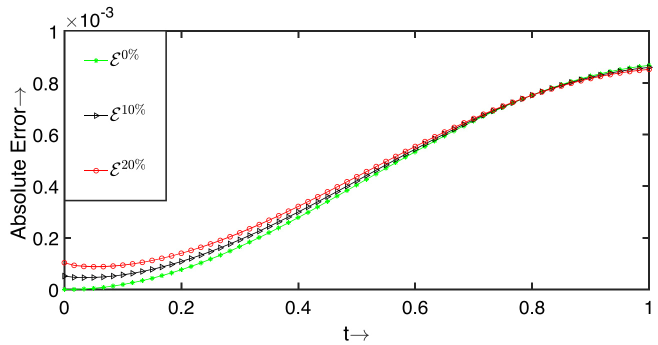

FIGURE 10 Absolute error with $\mathscr{M} = 60$ obtained via Scheme-I for Example 5.1. [Colour figure can be viewed at wileyonlinelibrary.com]

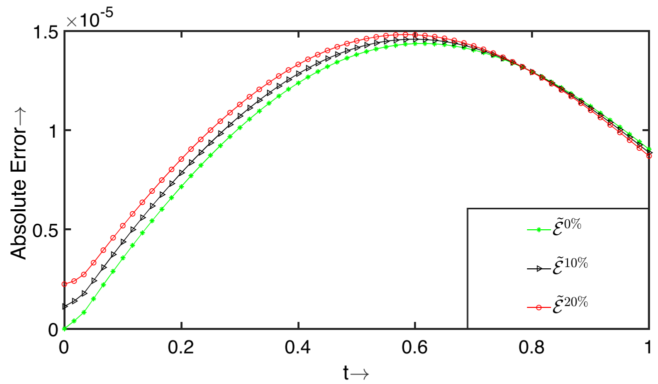

FIGURE 11 Absolute error with $\mathscr{M} = 60$ obtained via Scheme-II for Example 5.1. [Colour figure can be viewed at wileyonlinelibrary.com]

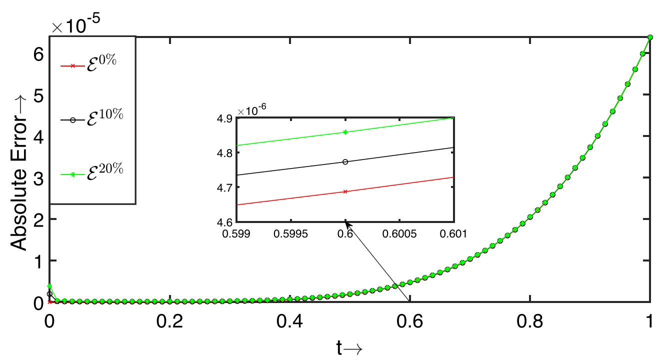

FIGURE 12 Absolute error for Example 5.2 obtained by Scheme-I with $\mathscr{M} = 80$. [Colour figure can be viewed at wileyonlinelibrary.com]

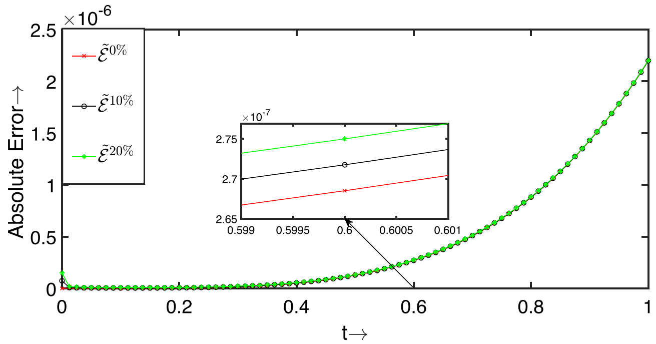

FIGURE 13 Absolute error for Example 5.2 obtained by Scheme-II with $\mathscr{M} = 80$. [Colour figure can be viewed at wileyonlinelibrary.com]

- Pointwise error, L_2-error, and maximum error for varying values of $\mathscr{M}$ and $\nu = 0.5$ with 10% noisy data are given in Table 8. Observe that after adding the 10% noisy data in the initial condition, there is a minimal difference in the numerical outcomes when compared with the numerical results obtained by the 0% noisy data in Table 7.
- Table 9 gives the pointwise error, L_2-error, and maximum error for various values of $\mathscr{M}$ and $\nu = 0.5$ with 20% noisy data. Observe that the variation in the numerical results obtained in this case is also almost negligible.
- From Tables 7, 8, and 9, it can be seen that after the slight perturbation of the initial condition, there is a very slight change in the obtained error results.
- Figure 10 shows the pictorial depiction of the variation of absolute error $\mathcal{E}^{0\%}$, $\mathcal{E}^{10\%}$, and $\mathcal{E}^{20\%}$ obtained by Scheme-I, with $\mathscr{M} = 60$ and $\nu = 0.5$.
- Graphical representation of absolute error $\tilde{\mathcal{E}}^{0\%}$, $\tilde{\mathcal{E}}^{10\%}$, and $\tilde{\mathcal{E}}^{20\%}$ obtained by Scheme-II, with $\mathscr{M} = 60$ and $\nu = 0.5$ is shown in Figure 11.
- From Figures 10 and 11 observe that the pictorial representation of absolute error shows that the effect of perturbation of the initial conditions in the pictorial representation is almost negligible.

The numerical results obtained for the second test problem are discussed below:

- Table 10 gives the pointwise error $\mathcal{E}^{0\%}$, $\tilde{\mathcal{E}}^{0\%}$ L_2-error, and maximum error $\Xi_{\mathscr{M}}$ for various values of $\mathscr{M}$ and $\nu = 0.2$ with 0% noisy data.
- Table 11 gives the pointwise error $\mathcal{E}^{10\%}$, $\tilde{\mathcal{E}}^{10\%}$ L_2-error, and maximum error $\Xi_{\mathscr{M}}$ for varying values of $\mathscr{M}$ and $\nu = 0.2$ with 10% noisy data.
- Table 12 gives the pointwise error $\mathcal{E}^{10\%}$, $\tilde{\mathcal{E}}^{0\%}$ L_2-error, and maximum error $\Xi_{\mathscr{M}}$ for various values of $\mathscr{M}$ and $\nu = 0.2$ with 20% noisy data.
- From these tables, it can be seen that after the slight perturbation of the initial condition there is very slight change in the error results obtained.
- Figure 12 shows the graphical representation of the absolute errors $\mathcal{E}^{0\%}$, $\mathcal{E}^{10\%}$, and $\mathcal{E}^{20\%}$ for $\mathscr{M} = 60$ with $\nu = 0.2$.
- Graphical representation of absolute errors $\tilde{\mathcal{E}}^{0\%}$, $\tilde{\mathcal{E}}^{10\%}$, and $\tilde{\mathcal{E}}^{20\%}$ are shown in Figure 13.
- From Figures 12 and 13 observe that the pictorial representation of absolute error shows that the effect of perturbation of the initial conditions in the pictorial representation is almost negligible.

7 | CONCLUDING REMARKS AND FUTURE WORK

In this manuscript L1, L1-2 discretization and the API method are used as a source for the numerical solution of FOVIDE (1.1). To obtain the approximate solution, two schemes are constructed. The first one is the scheme-I based on the L1 approximation with the API method of order $\mathcal{O}\left(h^{2-\nu}\right)$, while the second one is the scheme-II based on the L1-2 approximation with the API method of order $\mathcal{O}\left(h^{3-\nu}\right)$. Moreover, stability analysis and convergence analysis have been discussed. We additionally confirm the numerical stability of the proposed methods by introducing a disturbance into the initial condition. The effect of the disturbance is almost negligible in the numerical results, as shown by the error in Tables 7–12 and error graphs in Figures 10–13. As a result, it can be concluded that the techniques are stable numerically. Furthermore, numerical tests are conducted to check the efficiency and accuracy of the derived algorithms. The first example is to conduct a comparative study between the outcomes obtained from the designed methodology and those derived from the existing work [9]. From Tables 2 and 3, it is worth noting that the designed algorithms exhibited high accuracy with a better rate of convergence than in [9]. In addition, a second example is taken in which the kernel function has a weak singularity. The computational results were presented in Tables 4 and 5 and graphs in Figures 4–7, which confirm that the proposed approaches are also acceptable and more convenient for FOVIDE with weakly singular kernels. Also, by varying the parameter ν in the fractional derivative, the effect of this variation on the numerical outcomes can be observed graphically in Figures 2, 3, 6, and 7 via both schemes. From the above discussion, the idea of this technique can be further implemented to solve other mathematical models. For example, integral equations of non-integer order, differential equations of non-integer order, Fredholm integro-differential equations with nonlinear source terms of non-integer order, and many others are a future goal for the researchers.

AUTHOR CONTRIBUTIONS

Sunil Kumar: Methodology; formal analysis; writing—original draft. **Poonam Yadav:**Conceptualization; writing—review and editing; validation. **Vineet Kumar Singh:** Investigation; supervision; writing—review and editing.

ACKNOWLEDGEMENTS

The first author is grateful for the funding provided by the Senior Research Fellow (SRF) programme of the University Grants Commission (UGC), India, and the third author acknowledges the financial support from the Council of Science and Technology, U.P., under the project ID:1893.

CONFLICT OF INTEREST STATEMENT

The authors have no competing interests to declare that are relevant to the content of this article.

ORCID

Vineet Kumar Singh https://orcid.org/0000-0002-6220-9737

REFERENCES

1. H. Sun, Y. Zhang, D. Baleanu, W. Chen, and Y. Chen, *A new collection of real world applications of fractional calculus in science and engineering*, Commun. Nonlinear Sci. Numer. Simul. **64** (2018), 213–231.
2. D. A. Robinson, *The use of control systems analysis in the neurophysiology of eye movements*, Ann. Rev. Neurosci. **4** (1981), no. 1, 463–503.
3. R. Magin, *Fractional calculus in bioengineering, part 3*, Critical Rev. Biomed. Eng. **32** (2004), no. 3–4, 195–378.
4. I. Podlubny, *Fractional differential equations: an introduction to fractional derivatives, fractional differential equations, to methods of their solution and some of their applications*, Elsevier, 1998.
5. A. Kilbas, *Theory and applications of fractional differential equations*, Vol. **204**, Elsevier, 2006.
6. K. Diethelm and N. J. Ford, *The analysis of fractional differential equations*, Lect. Notes Math. **2004** (2010), 3–12.
7. R. C. MacCamy, *An integro-differential equation with application in heat flow*, Quart. Appl. Math. **35** (1977), no. 1, 1–19.
8. V. E. Tarasov, *Fractional integro-differential equations for electromagnetic waves in dielectric media*, Theor. Math. Phys. **158** (2009), 355–359.
9. B. Ghosh and J. Mohapatra, *Analysis of finite difference schemes for Volterra integro-differential equations involving arbitrary order derivatives*, J. Appl. Math. Comput. **69** (2023), no. 2, 1865–1886.
10. K. Diethelm and N. J. Ford, *Analysis of fractional differential equations*, J. Math. Anal. Appl. **265** (2002), no. 2, 229–248.
11. R. S. Das, *Theoretical prospects of fractional order weakly singular Volterra integro differential equations and their approximations with convergence analysis*, Math. Meth. Appl. Sci. **44** (2021), no. 11, 9419–9440.
12. L. S. Dong, N. V. Hoa, and H. Vu, *Existence and ulam stability for random fractional integro-differential equation*, Afrika Matematika **31** (2020), 1283–1294.
13. S. Santra, J. Mohapatra, P. Das, and D. Choudhuri, *Higher order approximations for fractional order integro-parabolic partial differential equations on an adaptive mesh with error analysis*, Comput. Math. Appl. **150** (2023), 87–101.
14. H. M. Srivastava, A. K. Nain, R. K. Vats, and P. Das, *A theoretical study of the fractional-order p-Laplacian nonlinear Hadamard type turbulent flow models having the Ulam–Hyers stability*, Revista de la Real Academia de Ciencias Exactas, Físicas y Naturales. Serie A. Mathematicas **117** (2023), no. 4, 160.
15. P. Das, S. Rana, and H. Ramos, *On the approximate solutions of a class of fractional order nonlinear Volterra integro-differential initial value problems and boundary value problems of first kind and their convergence analysis*, J. Comput. Appl. Math. **404** (2022), 113116.
16. R. Choudhary, S. Singh, P. Das, and D. Kumar, *A higher order stable numerical approximation for time-fractional non-linear kuramoto–sivashinsky equation based on quintic b b-spline*, Math. Meth. Appl. Sci. **117** (2024), 1–23.

17. P. Das, S. Rana, and H. Ramos, *Homotopy perturbation method for solving Caputo-type fractional-order Volterra-Fredholm integro-differential equations*, Comput. Math. Meth. **1** (2019), no. 5, e1047.
18. P. Das, S. Rana, and H. Ramos, *A perturbation-based approach for solving fractional-order Volterra-Fredholm integro differential equations and its convergence analysis*, Int. J. Comput. Math. **97** (2020), no. 10, 1994–2014.
19. K. Kumar, P. C. Podila, P. Das, and H. Ramos, *A graded mesh refinement approach for boundary layer originated singularly perturbed time-delayed parabolic convection diffusion problems*, Math. Meth. Appl. Sci. **44** (2021), no. 16, 12332–12350.
20. W. Jiang and T. Tian, *Numerical solution of nonlinear Volterra integro-differential equations of fractional order by the reproducing kernel method*, Appl. Math. Model. **39** (2015), no. 16, 4871–4876.
21. M. Akbar, R. Nawaz, S. Ahsan, K. S. Nisar, A.-H. Abdel-Aty, and H. Eleuch, *New approach to approximate the solution for the system of fractional order Volterra integro-differential equations*, Results Phys. **19** (2020), 103453.
22. A. Pedas, E. Tamme, and M. Vikerpuur, *Numerical solution of linear fractional weakly singular integro-differential equations with integral boundary conditions*, Appl. Numer. Math. **149** (2020), 124–140.
23. P. Yadav, B. P. Singh, A. A. Alikhanov, and V. K. Singh, *Numerical scheme with convergence analysis and error estimate for variable order weakly singular integro-differential equation*, Int. J. Comput. Meth. **20** (2023), no. 02, 2250046.
24. L. Zhu and Q. Fan, *Numerical solution of nonlinear fractional-order Volterra integro-differential equations by SCW*, Commun. Nonlinear Sci. Numer. Simul. **18** (2013), no. 5, 1203–1213.
25. M. H. Heydari, M. R. Hooshmandasl, F. Mohammadi, and C. Cattani, *Wavelets method for solving systems of nonlinear singular fractional Volterra integro-differential equations*, Commun. Nonlinear Sci. Numer. Simul. **19** (2014), no. 1, 37–48.
26. N. Rajagopal, S. Balaji, R. Seethalakshmi, and V. S. Balaji, *A new numerical method for fractional order Volterra integro-differential equations*, Ain Shams Eng. J. **11** (2020), no. 1, 171–177.
27. R. K. Maurya, V. Devi, N. Srivastava, and V. K. Singh, *An efficient and stable Lagrangian matrix approach to Abel integral and integro-differential equations,* Appl. Math. Comput. **374** (2020), 125005.
28. S. Santra and J. Mohapatra, *Numerical analysis of Volterra integro-differential equations with Caputo fractional derivative*, Iranian J. Sci. Technol., Trans. A: Sci. **45** (2021), no. 5, 1815–1824.
29. D. Shakti, J. Mohapatra, P. Das, and J. Vigo-Aguiar, *A moving mesh refinement based optimal accurate uniformly convergent computational method for a parabolic system of boundary layer originated reaction–diffusion problems with arbitrary small diffusion terms*, J. Comput. Appl. Math. **404** (2022), 113167.
30. P. Das, S. Rana, and J. Vigo-Aguiar, *Higher order accurate approximations on equidistributed meshes for boundary layer originated mixed type reaction diffusion systems with multiple scale nature*, Appl. Numer. Math. **148** (2020), 79–97.
31. P. Das, *An a posteriori based convergence analysis for a nonlinear singularly perturbed system of delay differential equations on an adaptive mesh*, Numer. Algorithms **81** (2019), no. 2, 465–487.
32. P. Das, *A higher order difference method for singularly perturbed parabolic partial differential equations*, J. Differ. Equ. Appl. **24** (2018), no. 3, 452–477.
33. P. Das, *Comparison of a priori and a posteriori meshes for singularly perturbed nonlinear parameterized problems*, J. Comput. Appl. Math. **290** (2015), 16–25.
34. B. Sikora, *Remarks on the Caputo fractional derivative*, Minut **5** (2023), 76–84.
35. C. Li and Z. Li, *Stability and ψ-algebraic decay of the solution to ψ-fractional differential system*, Int. J. Nonlinear Sci. Numer. Simul. **24** (2023), no. 2, 695–733.
36. A. Young, *Approximate product-integration*, Proc. Royal Soc. London. Ser. A. Math. Phys. Sci. **224** (1954), no. 1159, 552–561.
37. R. E. Beard, *Some notes on approximate product-integration*, J. Inst. Actuaries **73** (1947), no. 2, 356–416.
38. A. Young, *The application of approximate product-integration to the numerical solution of integral equations*, Proc. Royal Soc. London. Ser. A. Math. Phys. Sci. **224** (1954), no. 1159, 561–573.
39. Y. Lin and C. Xu, *Finite difference/spectral approximations for the time-fractional diffusion equation,* J. Comput. Phys. **225** (2007), no. 2, 1533–1552.
40. G. Gao, Z. Sun, and H. Zhang, *A new fractional numerical differentiation formula to approximate the Caputo fractional derivative and its applications*, J. Comput. Phys. **259** (2014), 33–50.
41. R. Shiromani, V. Shanthi, and P. Das, *A higher order hybrid-numerical approximation for a class of singularly perturbed two-dimensional convection-diffusion elliptic problem with non-smooth convection and source terms*, Comput. Math. Appl. **142** (2023), 9–30.
42. S. Saini, P. Das, and S. Kumar, *Computational cost reduction for coupled system of multiple scale reaction diffusion problems with mixed type boundary conditions having boundary layers*, Revista de la Real Academia de Ciencias Exactas, Físicas y Naturales. Serie A. Matemáticas, **117** (2023), no. 2, 66.
43. S. Saini, P. Das, and S. Kumar, *Parameter uniform higher order numerical treatment for singularly perturbed robin type parabolic reaction diffusion multiple scale problems with large delay in time*, Appl. Numer. Math. **196** (2024), 1–21.
44. M. Stynes, E. O Riordan, and J. L. Gracia, *Error analysis of a finite difference method on graded meshes for a time-fractional diffusion equation*, SIAM J. Numer. Anal. **55** (2017), no. 2, 1057–1079.

How to cite this article: S. Kumar, P. Yadav, and V. Kumar Singh, *Product integration techniques for fractional integro-differential equations*, Math. Meth. Appl. Sci. **48** (2025), 2833–2858, DOI 10.1002/mma.10464.

APPENDIX A

This section is dedicated to evaluating the performance of the proposed schemes for different variations in the model (1.1). Example A.1 is taken when the kernel function in the model (1.1) is considered to be negative, and Example A.2 corresponds to the case when coefficient of the fractional derivative in the model (1.1) is taken as 10^{-10}; in this case, it becomes singularly perturbed problem. We implemented the proposed schemes on these two examples, and the numerical results obtained are provided in Tables A1 and A2.

Example A.1. Consider the model (1.1) with negative kernel, $\mathcal{K}(t,s) = -(3t+4s)$, $\lambda = 1$, $\mathcal{A}(t) = 1$ under the initial condition $\mathcal{Y}(0) = 0$. We choose

$$\mathcal{G}(t) = \pi\nu \frac{(1+\nu)(2+\nu)(3+\nu)t^3 \csc(\pi\nu)}{6\Gamma(1-\nu)} + t^{3+\nu} - \frac{(7\nu+31)t^{5+\nu}}{(4+\nu)(5+\nu)},$$

so that analytical solution is $\mathcal{Y}(t) = t^{3+\nu}$. Now, following Algorithms 1 and 2 for this test problem, the maximum error and order of convergence obtained for different values of ν by Scheme-I and Scheme-II are given in Table A1.

After comparing the numerical results in Tables 1 and A1, it can be observed that, for a positive kernel, the error obtained by Scheme-I and Scheme-II is smaller than in the case of a negative kernel. However, the rate of convergence for Scheme-II with a negative kernel is slightly greater than with a positive kernel.

Example A.2. Consider the model (1.1) as

$$\begin{cases} 10^{-10}\mathcal{D}_t^{\nu}\mathcal{Y}(t) + \mathcal{A}(t)\mathcal{Y}(t) + \lambda \int_0^t \mathcal{K}(t,s)\mathcal{Y}(s)ds = \mathcal{G}(t), & t \in [0,T], \\ \mathcal{Y}(0) = a. \end{cases}$$

Let $\mathcal{K}(t,s) = (3t+4s)$, $\lambda = 1$, and $\mathcal{A}(t) = 1$ under the initial condition $\mathcal{Y}(0) = 0$. We choose

$$\mathcal{G}(t) = 10^{-10}\pi\nu \frac{(1+\nu)(2+\nu)(3+\nu)t^3 \csc(\pi\nu)}{6\Gamma(1-\nu)} + t^{3+\nu} + \frac{(7\nu+31)t^{5+\nu}}{(4+\nu)(5+\nu)},$$

so that analytical solution is $\mathcal{Y}(t) = t^{3+\nu}$.

TABLE A1 Comparison of $\Xi_{\mathscr{M}}$ and $\mathscr{C}_{\mathscr{M}}$ by using Scheme-II and Scheme-I with different values of ν and $\mathscr{M}$ for Example A.1.

		Scheme-I		Scheme-II	
ν	$\mathscr{M}$	$\Xi_{\mathscr{M}}$	$\mathscr{C}_{\mathscr{M}}$	$\Xi_{\mathscr{M}}$	$\mathscr{C}_{\mathscr{M}}$
0.2	32	1.6000e−03	-	6.2070e−05	-
	64	4.9704e−04	1.6866	9.5699e−06	2.6973
	128	1.5218e−04	1.7076	1.4518e−06	2.7207
	256	4.6048e−05	1.7246	2.1787e−07	2.7363
0.4	32	5.1000e−03	-	2.1891e−04	-
	64	1.8000e−03	1.5028	3.7758e−05	2.5355
	128	5.9841e−04	1.5888	6.4166e−06	2.5569
	256	2.0229e−04	1.5647	1.0804e−06	2.5702
0.6	32	1.2700e−02	-	6.1575e−04	-
	64	4.9000e−03	1.3740	1.2043e−04	2.3541
	128	1.9000e−03	1.3668	2.2340e−05	2.3735
	256	7.2945e−04	1.3811	4.4510e−06	2.3844
0.8	32	2.9300e−02	-	1.6000e−03	-
	64	1.2800e−02	1.1948	3.5621e−04	2.1673
	128	5.6000e−03	1.1926	7.8609e−05	2.1800
	256	2.5000e−03	1.1635	1.7234e−05	2.1894

TABLE A2 Comparison of $\Xi_{\mathscr{M}}$ and $\mathscr{C}_{\mathscr{M}}$ by using Scheme-II and Scheme-I with different values of ν and $\mathscr{M}$ for Example A.2.

		Scheme-I		Scheme-II	
ν	$\mathscr{M}$	$\Xi_{\mathscr{M}}$	$\mathscr{C}_{\mathscr{M}}$	$\Xi_{\mathscr{M}}$	$\mathscr{C}_{\mathscr{M}}$
0.2	16	5.3716e−09	-	5.3716e−09	-
	32	2.0165e−10	4.7354	2.0165e−10	4.7354
	64	9.5369e−12	4.4022	9.5469e−12	4.4007
	128	8.5243e−13	3.4839	7.7749e−13	3.6181
	256	4.4607e−12	2.3876	1.6473e−12	1.0832
0.4	16	4.9059e−09	-	4.9061e−09	-
	32	1.5591e−10	4.9757	1.5599e−10	4.9751
	64	6.4682e−12	4.5912	6.5327e−12	4.5776
	128	1.0961e−12	2.5610	1.9432e−12	1.7492
	256	2.8006e−12	1.3534	2.9909e−13	2.6998
0.6	16	2.8272e−09	-	2.8279e−09	-
	32	7.5724e−11	5.2225	7.6021e−11	5.2172
	64	2.5274e−12	4.9050	2.8031e−12	4.7613
	128	1.4859e−12	0.7663	1.6144e−12	0.7960
	256	2.6679e−12	0.8444	4.3626e−13	1.8877
0.8	16	1.0257e−09	-	1.0275e−09	-
	32	2.2433e−11	5.5148	2.3238e−11	5.4665
	64	4.5985e−13	5.6083	8.1245e−13	4.8381
	128	1.4252e−12	1.6319	1.5730e−12	0.9532
	256	4.3402e−12	1.6066	6.2828e−13	1.3240

Now, following Algorithms 1 and 2 for this test problem, the maximum error and order of convergence obtained for different values of ν by Scheme-I and Scheme-II are given in Table A2.

Initially, the error decreases as we increase the values of $\mathscr{M}$ for both schemes. However, beyond certain values of $\mathscr{M}$, the error starts increasing. Additionally, it can be observed from the table that there is a lot of variation in the rate of convergence.